GEORG-AUGUST-UNIVERSITÄT
GÖTTINGEN

MAX-PLANCK-GESELLSCHAFT

Bachelorarbeit am Max-Planck-Institut Göttingen
Abt. Dynamik komplexer Fluide

Simulationen von Fußgängerfluss und Streifenformation mithilfe kausaler Entropie

Simulations of Pedestrian Flow and Lane Formation through Causal Entropy

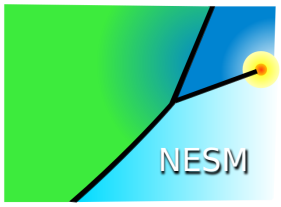

Florian Ebmeier

florian.ebmeier@stud.uni-goettingen.de

Erstgutachter: Dr. Marco G. Mazza
MPI für Dynamik und Selbstorganisation Göttingen
Dynamik komplexer Fluide

Zweitgutachter: Prof. Dr. Reiner Kree
Georg-August-Universität Göttingen
Institut für Theoretische Physik

Datum: 13. Januar 2017

Contents

Abstract

Simulating the dynamics of pedestrian flows is important for the design of safe public buildings and events. Due to the close connection between intelligent behaviour and pedestrian flows we propose a new simulation model using the causal entropic force model [1], which hints at a deeper connection between entropy maximization and intelligent behaviour.

We simulated pedestrians moving in opposite directions within a two-dimensional channel. These pedestrians are manipulated by the causal entropic force. In this study we were able to reproduce the phenomenon of lane formation, which is one of the basic phenomena of pedestrian dynamics.

In our simulations we were able to link the ratio R between the reservoir temperature and desired velocity to the formation of lanes. We also observed an ordering effect for large reservoir temperatures leading to fewer lanes formed.

We conclude that the causal entropic force acts as "intelligent noise" in our simulation models. These results give a good indication that the causal entropic force may be able to accurately model the dynamics of pedestrian flows.

1 Introduction

Figure 1: Pedestrians walking in different lanes along a corridor [2].

In this thesis we take a look at pedestrian dynamics and associated phenomena. One of the fundamental phenomena regarding pedestrian dynamics is the segregation into lanes of bilateral movement, which occurs in a plethora of different fields. We first describe lane formation and current simulation models thereof. Specifically, we want to look at the social force model, that simulates pedestrian movement [3]. Afterwards we introduce a new model proposing a connection between entropy maximization and intelligence [1].
This model has been used by Hornischer as a basis for some interesting simulations involving entropically driven particles [4]. As the concept of intelligent movement is inherently connected to the movement of pedestrians we propose using a variation of the causal entropic force model to simulate pedestrian flow. For this we will use Hornischer's simulation model as a basis and implement some of the aspects from the social force model to take a first step into simulating pedestrian movement through entropy maximization. Our goal in this thesis is to reproduce and analyse lane formation as encountered in pedestrian dynamics.

2 Lane formation

Lane formation is a state of movement where different lanes of uniform direction of movement form (see Fig. 1 & 2). It is a phenomenon that is associated with self-organization and optimization of movement [5]. We first list different contexts in which lane formation is observed and then take a look at the optimization of movement through lane formation.

2.1 Lane formation in different contexts

Lane formation is a widely analysed phenomenon and is encountered in a plethora of different contexts. It is observed in the behaviour of army ants [6], pedestrian flow or oppositely charged colloids [7, 8], as well as ionic conductors in an electric field [9]. Here we want to study lane formation as an emergent behaviour with and without an external field.

In a system of oppositely charged colloids [7, 8] lane formation can emerge as a consequence of an external electric field. The colloids can be viewed as two types of Brownian colloidal particles that interact with each other according to an effective, screened Coulomb interaction. In that work it was concluded that lane formation was a very general process. It was observed for oscillating electric fields and both in two and three spatial dimensions [7, 8].

Lane formation was also observed in the movement of army ants. Army ants secrete pheromones during their motion that thus form long chemical trails which are densely populated with ants. These ants were simulated [6] to follow the chemical trails of the other ants similarly to chemotaxis. That model mostly explored the effect of turning rates and local perception on traffic flows. In simulations bilateral movement as well as lane formation was observed and analysed. It was found that the behaviour of army ants exhibits optimal parameters, which leads to maximized traffic flow [6].

2.2 Lane formation as optimizing state

Lane formation is a non-trivial aspect of self-organized movement. Let us consider a set of particles with opposite preferred direction of movement and repulsive interaction between particles. Consider the position $\boldsymbol{x}_i(t)$ of particle i at time t , its velocity $\boldsymbol{v}_i(t)$, v_0 its target speed and $\hat{\boldsymbol{e}}_i$ its preferred direction of motion. The equation of

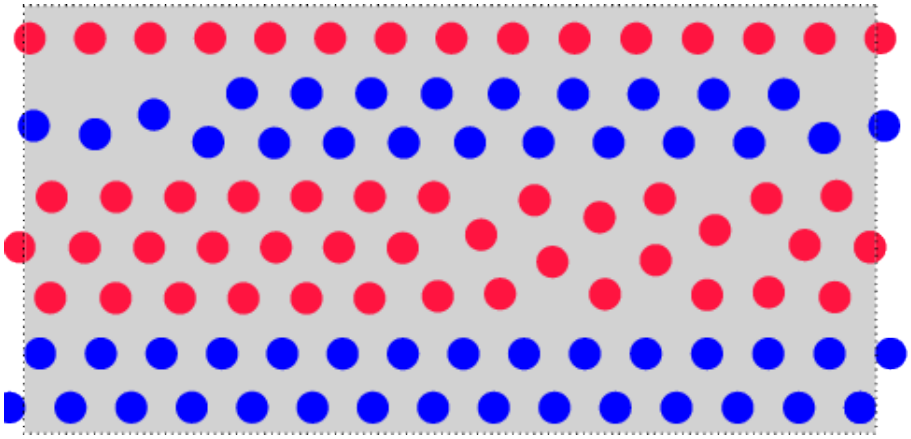

Figure 2: Particles of opposite preferred direction of movement showing lane formation [5]. Different colors represent different moving directions.

motion can then be written quite generally as

$$\boldsymbol{v}_i = v_0 \hat{\boldsymbol{e}}_i + \sum_{j(\neq i)} \boldsymbol{f}_{ij}(\boldsymbol{d}_{ij}(t)), \tag{1}$$

where $\boldsymbol{f_{ij}}$ is the repulsive interaction between different particles. We also assume that this interaction decreases monotonically with increasing distance $\boldsymbol{d}_{ij}$ between both particles. We can now quantify the efficiency as

$$E = \frac{\langle \langle \boldsymbol{v}_i \cdot \hat{\boldsymbol{e}}_i \rangle_i \rangle_t}{v_0} \leq 1, \tag{2}$$

which describes the average fraction of the desired velocity with which the particle approaches its destination. An efficiency close to 1 will thus denote a state of movement in most particles approach their destinations with their target speed, while an efficiency close to 0 denotes a state of movement where particles do not approach their destination at all. Lane formation maximizes this quantity. The optimization of efficiency also implies the minimization of interaction intensity.

$$\left\langle \left\langle - \sum_{i,j(j\neq i)} \boldsymbol{f}_{ij} \cdot \hat{\boldsymbol{e}}_i \right\rangle_i \right\rangle_t = v_0 - \langle \langle \boldsymbol{v}_i \cdot \boldsymbol{e}_i \rangle_i \rangle_t = v_0(1 - E). \tag{3}$$

Particles moving with opposite directions in the same lane will collide very frequently, and thus contribute with a large interaction energy. Lane formation minimizes the interaction rate and thus is, in a system of opposite preferred directions, an optimal self-organized steady state (see [3, 5] for a derivation).

3 Pedestrian flows

Before we look at lane formation in the context of pedestrian flow we want to take a look at the general phenomenology observed in pedestrian flow. Here we want to separate normal pedestrian behaviour from panic behaviour.

3.1 Normal behaviour

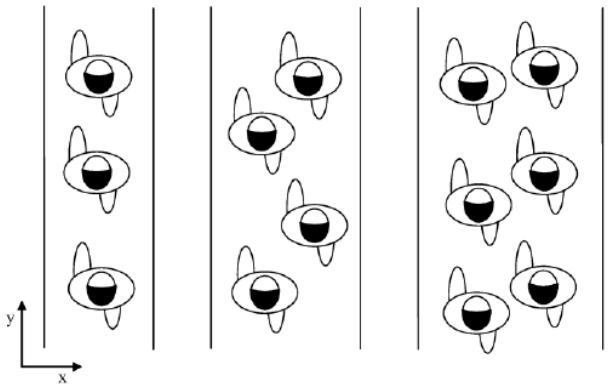

Figure 3: Sketch of pedestrians walking in a bottleneck, showing zipper effect [10].

.

In a study of pedestrian behaviour at bottlenecks with unilateral flow, Hoogendorn and Daamen [11] found that pedestrians, under saturated conditions, form layers dynamically. These layers have lateral distances between them that are lower than the average shoulder width of pedestrians. This leads to an effect coined the "zipper" effect (see Fig. 3). The headway distance between pedestrians, the distance between one pedestrian and the pedestrian in front of it, was observed to fluctuate around a constant value throughout the entire layer. These findings lead to the conclusion that layers merge together and move at the same speed [11].

At intermediate and high densities pedestrian crowds behave very similarly to gases, fluids and granular flows. This similarity is apparent in different phenomena of pedestrian movement. For example, Helbing likens the tracks of pedestrians in snow to streamlines of fluids [12]. At the interface between opposite walking directions phenomena similar to "viscous fingering" is observed [13]. Segregation into lanes of uniform walking directions occurs similarly to phenomena of segregation and stratification in granular matter. Another similarity is the oscillation of passing direction at bottlenecks [14], which can be compared to the "saline oscillator" [15]. For a more detailed comparison between the behaviour of pedestrian crowds and gases, fluids and granular flows see [12].

Other phenomena observed in pedestrian flow in non-panic situations include:

- Pedestrians tend to take the fastest route, which does not necessarily have to be the shortest. Pedestrians also seem to minimize the effort associated with taking a certain path [16]. Their ways can be accurately approximated through polygons [3].

- A pedestrians desired speed corresponds to the least energy consuming walking speed. The desired walking speed is Gaussian distributed with an average of 1.34m/s and a standard deviation of 0.26m/s [17, 18].

- The distance between pedestrians and obstacles, such as other pedestrians or walls, decreases with increasing density and higher desired walking speed [19].

- Pedestrians at rest are uniformly distributed over the entire available area, with pedestrian density increasing around "attractive" places, such as street vendors. Acquainted individuals may form groups, which in turn behave like a single pedestrian. The size of such groups are Poisson distributed [20, 21].

3.2 Panic situations

Panic situations usually occur at mass gatherings. While sometimes the reason for panic to erupt can be apparent, as in the case of a fire or other life threatening situations [22, 23], panics seemingly also occur for no discernible reason at all. The resulting stampedes often lead to people being crushed or trampled down. While experiments involving panic behaviour are difficult because of the obvious ethical concerns, the analysis of panic disasters has yielded some information on the behaviour of panicking crowds. We now take a look at the observed behaviour of pedestrians in panic and escape situations.

- During panic situations individual pedestrians try to move faster and overtake others [24].

- Traversing bottlenecks becomes increasingly uncoordinated and jams build up at bottlenecks and, in particular, exits [25]. These jams at exits can lead to clogging and arching, making the exits nearly intraversable [24]. This behaviour is similar to the flow of rough granular matter through small openings [12].

- The interaction in crowds leads to pressure buildups, which lead to extreme pressures of up to 4500 Newtons per meter [23, 26].

- Pedestrians in panic situations will adopt herding behaviour, and overlook or inefficiently use alternative exits [22].

3.3 Social force model

To simulate pedestrian dynamics Helbing introduced the social force model for pedestrian dynamics [3, 14]. In this model it is assumed that every pedestrian wants to move with a desired speed v_i^0 in a desired direction $\boldsymbol{e}_i^0$. If the actual speed of the pedestrian deviates from the desired speed, the pedestrian will experience a restoring force with relaxation time τ

$$\boldsymbol{F}_i^0 = \frac{1}{\tau}(v_i^0 \boldsymbol{e}_i^0 - \boldsymbol{v}_i). \tag{4}$$

Here $\frac{1}{\tau} v_i^0 \boldsymbol{e}_i^0$ can be seen as an acceleration term while $\frac{1}{\tau}\boldsymbol{v}_i$ is equivalent to a friction term.

The social force model also assumes a repulsive force between two pedestrians i and j that becomes increasingly large as they approach each other.

$$\boldsymbol{f}_{i,j}^{soc}(t) = A_i \exp[(r_{ij} - d_{ij})/B_i]\boldsymbol{n}_{ij}\left(\lambda_i + (1-\lambda_i)\frac{1+\cos(\phi_{ij})}{2}\right), \tag{5}$$

where A_i the interaction strength, B_i the range of the repulsive force, d_{ij} the distance between the centers of mass of pedestrians i and j, and r_{ij} the sum of their radii. $\boldsymbol{n}_{ij}$ denotes the normalized connection vector pointing from pedestrian i to pedestrian j. Setting $\lambda_i < 1$ leads to the anisotropic behaviour of pedestrian interaction, i.e. the interaction with the front neighbour of the pedestrian has a higher impact on its behaviour. The social force model includes time-dependent attractive interactions towards special 'attractions', and acquainted individuals. For simplicity these effects as well as anisotropic behaviour were dropped in [3].

For panicking individuals, physical interaction also plays a role and a "body-force" counteracting compression as well as a "sliding friction force" for tangential friction is introduced

$$\boldsymbol{f}_{ij}^{ph} = k\Theta(r_{ij} - d_{ij})\boldsymbol{n}_{ij} + \kappa\Theta(r_{ij} - d_{ij})\Delta v_{ji}^t \boldsymbol{t}_{ij}, \tag{6}$$

where $\Theta(z) = z$ for $z \geq 0$ and 0 otherwise, $\boldsymbol{t}_{ij}$ denotes the tangential direction while Δv_{ji}^t is the tangential velocity. κ and k represent large constants to reasonably scale the forces.

3.3.1 Phenomenology of the social force model

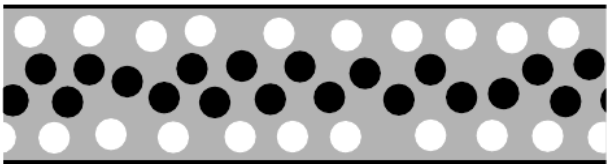

Figure 4: Lane formation as observed in [3]. Different colors represent different moving directions.

The social force model has reproduced the empirically observed phenomenon of lane formation (see fig. 4). In this simulation we see the "zipper" effect observed in [11], as the outer lanes restrict the available space and form a bottleneck for the center layer. These simulations also observed a "noise-induced ordering", which increases segregation of lanes with medium noise amplitude in contrast to small noise amplitude. Further increasing of the noise amplitude leads to a blocking phase transition that Helbing coins "freezing by heating" [27]. By increasing the fluctuation strength, which the author suggests as equivalent to temperature, at sufficiently high densities, lanes were broken up and a phase transition was observed (see figure 5). In contrast to the expected disordered state, equivalent to a "gaseous" state, the system assumed a locked state, similar to a solid. This "freezing by heating" effect was attributed by Helbing to the driving term as well as the dissipative friction.

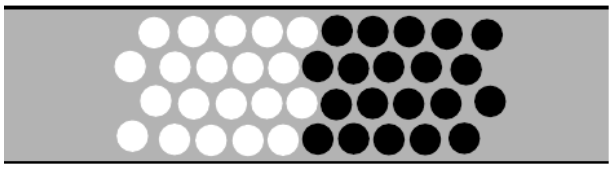

Figure 5: Blocking transition induced by noise [3]. Different colors represent different moving directions.

Simulations of bilateral movement at bottlenecks show the oscillation of the moving direction in non-panic situations. A pedestrian that moves through the bottleneck leads to pedestrians with the same walking direction to easily pass through. If, because of a fluctuation, the number of pedestrians on one side drops, the resulting pressure also drops, which allows particles moving in the opposite walking direction to get a chance at occupying the passage (see fig.6). Dynamics at intersections with more than two preferred directions of movement hold short-lived and unstable patterns of motion [3, 28].

In panic situations both the level of fluctuations and the desired velocity increase [24]. It is also assumed that panicking individuals are more likely to do what other

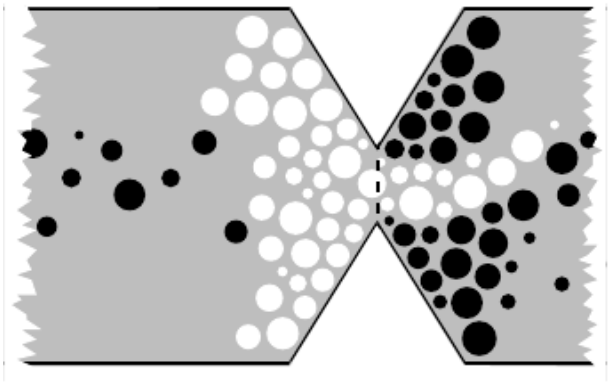

Figure 6: Oscillation of passing direction at bottleneck [3]. Different colors represent different moving directions.

people do. An additional herding interaction was implemented in [3] to simulate this effect.

The simulations have also shown clogging as well as arching for desired velocities over 1.5 m/s, which is consistent with observations. This leads to the "faster is slower" effect. Since a higher desired velocity leads to clogging and arching in certain conditions, it can lead to a lower average speed. This is highly dependent on the friction parameter κ. The "faster is slower" effect sets in through a combination of clogging due to bottlenecks and strong friction. Helbing proposes that this can be minimized by avoiding bottlenecks in construction [3, 28]. He further advises that the widening of escape routes will lead to a similar effect, with a stronger effect in case of narrow corridors, high or different desired velocities and high densities.

Helbing also proposes a change in velocity dependent on a nervousness parameter to simulate panics without a definite source. Here small fluctuations in velocity can lead to a feedback loop causing high desired velocities, that thus create panic. Further adjustments to the model have been made to account for different situations. One would be the evacuation of a smoke filled room, where exits have to be found first. Here Helbing proposes a preferred direction dependent on those of other pedestrians around it and a nervousness factor.

In conclusion the model reproduces many different phenomena of pedestrian dynamics. For numerous panic situations the model has to be expanded and there is a large amount of different forces acting on the pedestrian. We now want discuss the concept of causal entropic force to motivate a simulation model based on entropy maximization.

4 Causal entropic force

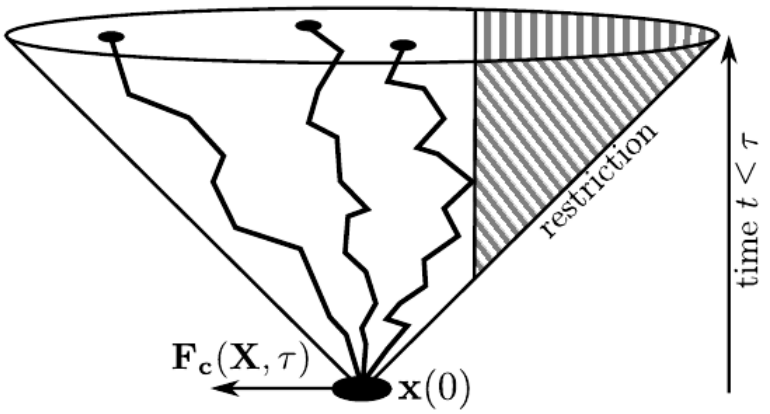

Figure 7: Light-cone representing phase space with causal entropic force driving the system away from the restricted area [4].

The concept of entropy maximization has been used in different fields such as cosmology, geophysics and computer science [29–33]. Research in these fields has hinted at a possible connection between entropy maximization and intelligence. A first step towards a formal physical relationship between these two has been proposed in a paper by Wissner-Gross and Freer [1]. Starting from the general entropic force they proposed a system that does not maximize immediate entropy production, but rather maximize entropy production between the present state and a future time horizon.

Figure 7 shows the different states a system can reach within the time interval $[0, \tau]$. If a part of this phase space is restricted, the causal entropic force will maximize the amount of states the system can evolve into. Consequently the causal entropic force will push the system away from restricted states.

4.1 Formal derivation

We start from a classical entropic force $\boldsymbol{F}$ in a canonical ensemble

$$\boldsymbol{F}(\boldsymbol{X}_0) = T\nabla_{\boldsymbol{X}} S(\boldsymbol{X})|_{\boldsymbol{X}_0}, \tag{7}$$

where T is the reservoir temperature, $S(\boldsymbol{X})$ the entropy associated with macrostate $\boldsymbol{X}$ and the current macrostate $\boldsymbol{X}_0$. Instead of maximizing the instantaneous entropy production Wissner-Gross and Freer [1] associated the causal path entropy of macrostate $\boldsymbol{X}$ with all possible phase-space paths in a finite time interval $[0, \tau]$.

The causal path entropy S_c of macrostate $\boldsymbol{X}$ can then be written as the path integral

$$S_c(\boldsymbol{X}, \tau) \equiv -k_B \int_{\boldsymbol{X}(t)} Pr(\boldsymbol{\chi}_\tau|\boldsymbol{x}(0)) \ln Pr(\boldsymbol{\chi}_\tau|\boldsymbol{x}(0)) \mathcal{D}\boldsymbol{\chi}_\tau \tag{8}$$

with $Pr(\boldsymbol{\chi}_\tau|\boldsymbol{x}(0))$ is the conditional probability for the system to evolve through path $\boldsymbol{\chi}_\tau$ given the initial system state $\boldsymbol{x}(0)$. This probability equates the integral over all possible paths taken by the open system's environment during the time interval $[0, \tau]$

$$Pr(\boldsymbol{\chi}_\tau|\boldsymbol{x}(0)) = \int_{\boldsymbol{\xi}} Pr(\boldsymbol{\xi}_\tau|\boldsymbol{x}(0)) \mathcal{D}\xi. \tag{9}$$

The resulting causal entropic force is then

$$\boldsymbol{F}_c(\boldsymbol{X}_0, \tau) = T_c \nabla_{\boldsymbol{X}} S_c(\boldsymbol{X}, \tau)|_{\boldsymbol{X}_0} \tag{10}$$

with causal path temperature T_c, which determines the tendency of the system to evolve to a macrostate of higher causal entropy. Assuming position coordinates $q_j(0)$, we can rewrite this as

$$\boldsymbol{F}(\boldsymbol{X}_0, \tau) = T_c \frac{\partial S_c(\boldsymbol{X}_0, \tau)}{\partial q_j(0)}. \tag{11}$$

Using equation 8 this comes to

$$\boldsymbol{F}(\boldsymbol{X}_0, \tau) = -T_c k_b \int \frac{\partial Pr(\boldsymbol{\chi}_\tau|\boldsymbol{x}(0))}{\partial q_j(0)} \ln[Pr(\boldsymbol{\chi}_\tau|\boldsymbol{x}(0))] \mathcal{D}\boldsymbol{\chi}_\tau. \tag{12}$$

We assume the environment of our system to be a heat reservoir with reservoir temperature T_r, which rethermalizes the forced degrees of freedom at a timescale ϵ. This rethermalization is assumed to happen via nonlinear Langevin dynamics with

temporally discretized additive thermal noise as well as friction terms (compare [1]). Under this assumption the system is deterministic within the interval $[t, t+\epsilon]$ and thus we can rewrite any non-zero conditional path probability as the product of the probabilities of its intervals

$$Pr(\boldsymbol{\chi}_\tau|\boldsymbol{x}(0)) = \left[\prod_{n=1}^{N} Pr(\boldsymbol{x}(t_{n+1})|\boldsymbol{x}(t_n))\right] Pr(\boldsymbol{\chi}_\epsilon|\boldsymbol{x}(0)). \tag{13}$$

Where $t_n = n\epsilon$ and $N = \tau/\epsilon$. We can write the gradient as

$$\frac{\partial Pr(\boldsymbol{\chi}_\tau|\boldsymbol{x}(0))}{\partial q_j(0)} = \left[\prod_{n=1}^{N} Pr(\boldsymbol{x}(t_{n+1})|\boldsymbol{x}(t_n))\right] \frac{\partial Pr(\boldsymbol{\chi}_\epsilon|\boldsymbol{x}(0))}{\partial q_j(0)}. \tag{14}$$

We now choose ϵ to be smaller than any kinetic or spatial variation of internal system forces $h(x)$

$$\epsilon \ll \sqrt{\frac{2m_j}{|\nabla_{\boldsymbol{q}(0)} h_j(\boldsymbol{x}(0))|}}, \tag{15}$$

$$\epsilon \ll \sqrt{\frac{1}{|\nabla_{\boldsymbol{p}(0)} h_j(\boldsymbol{x}(0))|}}. \tag{16}$$

Therefore we can Taylor expand $q_j(\epsilon)$

$$q_j(\epsilon) = q_j(0) + \frac{p_j(0)}{2m_j}\epsilon + \frac{f_j(0) + h_j(0)}{2m_j}\epsilon^2, \tag{17}$$

with $f_j(t)$ as a random Gaussian force.

$$\langle f_j(t)\rangle = 0 \tag{18}$$

$$\langle f_j(t) f_{j'}(t')\rangle = \frac{m_j k_B T_r}{\epsilon^2}\delta_{ij}\delta(t-t') \tag{19}$$

From this we can conclude that $Pr(\boldsymbol{\chi}_\epsilon|\boldsymbol{x}(0))$ is Gaussian in $q_j(\epsilon)$ and

$$Pr(\boldsymbol{\chi}_\epsilon|\boldsymbol{x}(0)) \sim \exp\left(-\frac{1}{2}\frac{(q_j(\epsilon) - \langle q_j(\epsilon)\rangle)^2}{\langle q_j^2(\epsilon)\rangle - \langle q_j(\epsilon)\rangle^2}\right) \tag{20}$$

$$= \frac{(q_j(\epsilon) - \langle q_j(\epsilon)\rangle)^2}{\langle q_j^2(\epsilon)\rangle - \langle q_j(\epsilon)\rangle^2} Pr(\boldsymbol{\chi}_\epsilon|\boldsymbol{x}(0)) \tag{21}$$

$$= \frac{2f_j(0)}{k_B T_r} Pr(\boldsymbol{\chi}_\epsilon|\boldsymbol{x}(0)) \tag{22}$$

Using this we can simplify equation (12) to

$$\boldsymbol{F}(\boldsymbol{X}_0, \tau) = -\frac{2T_c}{T_r} \int \boldsymbol{f}_j(0) Pr(\boldsymbol{\chi}_\tau | \boldsymbol{x}(0)) \ln[Pr(\boldsymbol{\chi}_\tau | \boldsymbol{x}(0))] \mathcal{D}\chi_\tau. \tag{23}$$

For a more detailed derivation see [1, 4].

4.2 Simulation results

Wissner-Gross and Freer used this concept to test the causal entropic force model in four different simple scenarios [1]. They simulated a particle in a 2 dimensional box and let the 2 degrees of freedom evolve via the causal entropic force. This has lead the particle to move to the center of the box.

In similar fashion, an inverted pendulum is manipulated through a causal entropy driven cart. The simulation has shown that the causally entropy driven cart will manipulate the pendulum to an upright position and attempt to balance it there, as this is the position with maximum causal entropy.

For a third example a tool-use puzzle, based on puzzles used for animals, was used. Here a disk subject to causal entropic forcing used a disk simulating a tool to free a third object from an enclosure too narrow to reach. A fourth system has shown social cooperation in two socially forced agents freeing a bigger disk to allow direct manipulation. These last two simulations have shown similarities to cognitive behaviour, showing a good first step in the connection between intelligent behaviour and entropy maximization.

5 Simulation model

As a basis to our simulations we take Hornischer's simulation model [4] and try to apply it to pedestrian dynamics. As described by Helbing in [3] a model that simulates pedestrian dynamics should always reproduce the phenomenon of lane formation in order to be realistic. For this we take the concepts of desired velocity v_0 and direction $\boldsymbol{e}_0$ from the social force model and apply them to Hornischer's model of entropically driven particles. We take the friction and acceleration term from the social force model and replace all social force terms with the causal entropic force.

5.1 Calculation of the causal entropic force

To calculate the causal entropic force we need to sample the probability $Pr(\boldsymbol{\chi}_\tau|\boldsymbol{x}(0))$. We use M Brownian trajectories starting from the current state $\boldsymbol{x}_0$ with a finite time horizon of τ. We then assign a phase space volume Ω_i to each trajectory

$$\Omega_i \propto \frac{1}{Pr(\boldsymbol{\chi}_{\tau i}|\boldsymbol{x}(0))}. \tag{24}$$

Normalization then implies

$$\sum_i^M \Omega_i Pr(\boldsymbol{\chi}_{\tau i}|\boldsymbol{x}(0)) = 1, \tag{25}$$

$$\Omega_i = \frac{1}{MPr(\boldsymbol{\chi}_{\tau i}|\boldsymbol{x}(0))} \tag{26}$$

Using this in Eq. 23 :

$$\boldsymbol{F}_j(\boldsymbol{X}_0,\tau) = -\frac{2T_c}{T_r}\int \boldsymbol{f}_j(0) Pr(\boldsymbol{\chi}_\tau|\boldsymbol{x}(0)) \ln[Pr(\boldsymbol{\chi}_\tau|\boldsymbol{x}(0))]\mathcal{D}\chi_\tau \tag{27}$$

$$\approx -\frac{2T_c}{T_r}\langle\sum_i \boldsymbol{f}_{ij}(0)\frac{1}{M\Omega_i}\ln\left(\frac{1}{M\Omega_i}\right)\Omega_i\rangle \tag{28}$$

$$= \frac{2T_c}{T_r M}\langle\sum_i \boldsymbol{f}_{ij}(0)\ln(M\Omega_i)\rangle \tag{29}$$

$$= \frac{2T_c}{T_r M}\langle\sum_i \boldsymbol{f}_{ij}(0)\ln(\Omega_i)\rangle \tag{30}$$

Adding a vanishing term will yield

$$\boldsymbol{F}_j(\boldsymbol{X}_0, \tau) = \frac{2T_c}{T_r M} \langle \sum_i \boldsymbol{f}_{ij}(0) \ln \left(\frac{\Omega_i}{\langle \Omega_{i'} \rangle} \right) \rangle. \tag{31}$$

As in Hornischer's simulations [4] we choose the radius of gyration to quantify the phase space volume Ω_i:

$$R_i = \frac{1}{M} \sum_{k=1}^{M} (\boldsymbol{r}_k - \boldsymbol{r}_{mean})^2 \tag{32}$$

With $M = \frac{\tau}{\delta t}$ as the number of steps per sampling path.

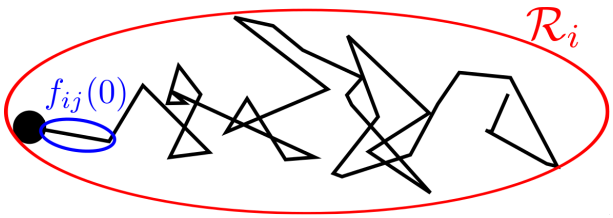

Figure 8: Schematic of trajectory including first step (blue ellipse) and radius of gyration used as weight for Ω_i (red ellipse) [4].

A trajectory closer to an obstacle or restricted phase space will be more likely to fold and thus be statistically smaller, while a trajectory in open space will more likely be elongated. This leads to a good quantification of the phase space volume, given a large enough number of sampling paths. The force at time $t = 0$ $\boldsymbol{f}_{ij}$ for the trajectory is given through the first step of the trajectory.

5.1.1 Implementation

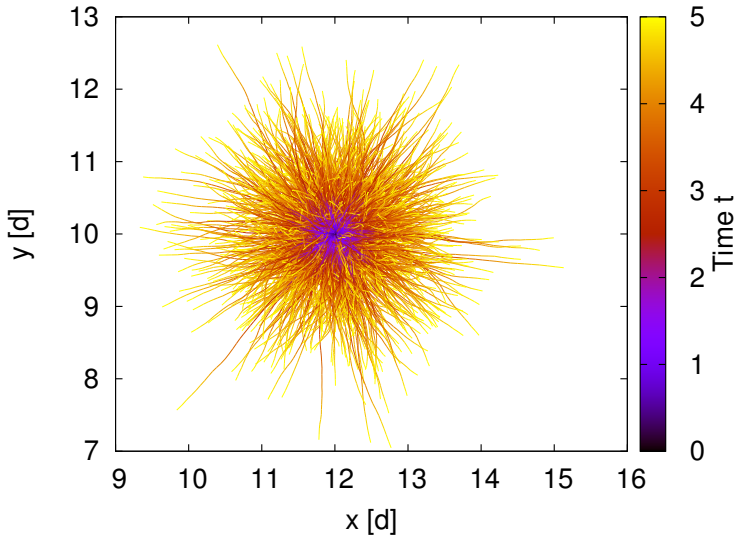

Figure 9: Example for the trajectory horizon with no desired velocity v_0. Parameters: 2500 trajectories, $T_r = 0.0001$, $v_0 = 0.00$, $\tau = 2.5$, $\delta t = 0.1$.

The Brownian sample trajectories evolve according to the Langevin equation:

$$m\dot{\boldsymbol{v}} = \boldsymbol{\xi}(t) + \boldsymbol{h}(\boldsymbol{x}) \tag{33}$$

with mass $m = 1$, $\boldsymbol{h}(\boldsymbol{x})$ representing external forces, such as walls or other pedestrians, and $\boldsymbol{\xi}$ as Gaussian noise. The first step as well as the radius of gyration of every trajectory is used to calculate the causal entropic force. The parameters of τ and δt define the total number of timesteps. Here we have to choose the parameters carefully, as with too large a number of steps the first step loses influence over the trajectory and for significant results a very large number of sample trajectories is needed [4]. An example of those trajectories and the resulting horizon can be seen in figure 9. It is also noted that a trajectory colliding with a particle will treat this particle like a wall and reflect off the particle. During the simulation of sample trajectories other particles are assumed to move at their current speed in the same direction they are currently moving in. Thus the trajectories will not collide with particles moving away from them at a higher speed than themselves.

5.2 Equations of motion

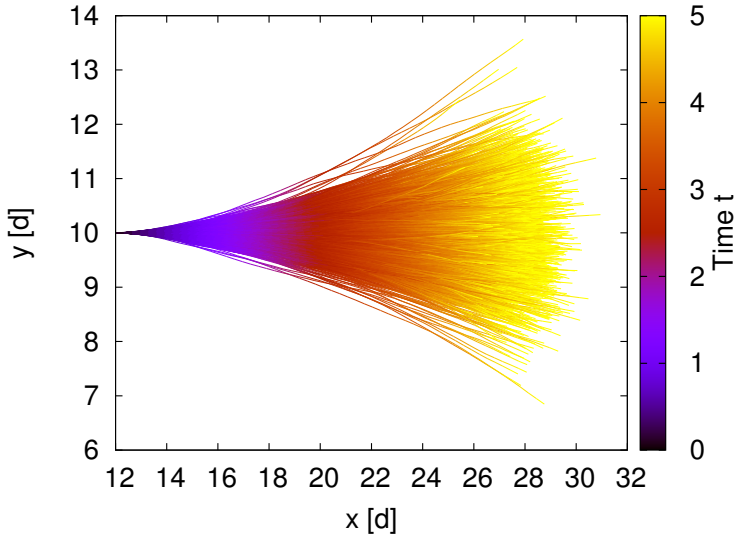

Figure 10: Example for the trajectory horizon with desired velocity v_0. Parameters: 2500 trajectories, $T_r = 0.0001$, $v_0 = 3.2d/s$, $\tau = 2.5$, $\delta t = 0.1$.

Our entropically driven particles obey the following equation of motion:

$$m\dot{\boldsymbol{v}} = \boldsymbol{F}_C(t) + \boldsymbol{h}(t) + \frac{v_0\boldsymbol{e}_0 - \boldsymbol{v}}{t_{rel}} \tag{34}$$

with causal entropic force $\boldsymbol{F}_C(t)$ and external forces $\boldsymbol{h}(t)$. We included the driving term $\frac{1}{t_{rel}}v_0\boldsymbol{e}_0$ and the dissipative friction term $\frac{-1}{t_{rel}}\boldsymbol{v}$ from the social force model to simulate the pedestrians tendency to reach the desired velocity v_0 as well as direction of motion $\boldsymbol{e}_0$ within a certain time frame t_{rel}. Once pedestrians get close enough to touch each other they experience a repulsive force through a harmonic force $\boldsymbol{H}_{ij}$

$$\boldsymbol{H}_{ij} = -Ku(r_{ij} - d)\hat{\boldsymbol{n}}_{ij}, \tag{35}$$

with the diameter of pedestrians d, the distance between pedestrian i and pedestrian j, r_{ij} and the normalized connection vector between both pedestrians $\boldsymbol{n}_{ij}$. The function $u(z)$ is 0, if its argument is below 0 and equals its argument if it is above 0. This force is not present in the virtual trajectories used to calculate the causal entropic force, as pedestrians will bounce off each other in that case. The resulting direction of movement and desired velocity also influence the trajectory horizon, as pedestrians tend to have a large velocity in comparison to the Brownian noise used to calculate the causal entropic force.

Instead of a nearly circular envelop of the sampling trajectories as in figure 9 this results in a cone shaped horizon as in figure 10. This results in an anisotropic

pedestrian interaction similar to the consequences of parameter $\lambda_i < 1$ in the social force model (section 3.3).

5.2.1 Interaction range

We can now take a closer look at the interaction range that the trajectory horizon generates. Assuming our pedestrian moves at desired velocity v_0 it will keep moving in the same direction with that velocity along the virtual trajectories. This will result in a total distance of $s_v = \tau v_0$. The Brownian trajectories themselves have an average distance from their starting point

$$s_t = \sigma\sqrt{\tau dt}, \tag{36}$$

with $\sigma = \frac{mk_BT_r}{dt^2}$. The mass is set to $m = 1$ and the Boltzmann constant is set to $k_B = 1$. Assuming the Brownian trajectory has a net displacement from its start and moves along the direction of movement the pedestrian has, we can write the displacement as

$$s = \tau v_0 + \frac{T_r k_B}{dt^2}\sqrt{dt\tau}. \tag{37}$$

This gives us an indicator of the interaction range. It is noted, though, that the displacement of the Brownian trajectories can be larger, thus the real interaction range will be larger than s.

5.2.2 Parameter influences and boundary conditions

First we define the diameter d of one pedestrian as our standard unit of length. With this all our spacial parameters will be given in units of d. In our simulation we want to reproduce lane formation and thus choose our boundary conditions accordingly. We simulate pedestrians in a two-dimensional channel of length $40d$ and height $20d$. With hard walls in the y-direction and periodic boundary conditions in x-direction. Every simulated pedestrian is randomly assigned with a desired direction of motion along the x-axis, either $\boldsymbol{e}_i^0 = \boldsymbol{e}_x$ or $\boldsymbol{e}_i^0 = -\boldsymbol{e}_x$, with equal probability. Thus we create bilateral movement of pedestrians inside a channel, which should result in lane formation, given the right density, reservoir temperature and desired velocity. In table 1 we collect all the simulation parameters and their physical significance.

N	Pedestrian movement is strongly dependent on the density and the amount of simulated pedestrians N. Assuming our boundary conditions of height $20d$ and length $40d$ the density is $\rho = \frac{N}{800d^2}$.
T_r	Increasing the reservoir temperature T_r increases the step size of sampling trajectories. This results in a larger interaction range as well as a higher total causal entropic force.
T_c/T_r	Inspecting eq.31 it is apparent that this parameter linearly affects the magnitude of the causal entropic force. In our simulations this value is at a constant $T_c/T_r = 5$.
τ and δt	These parameters influence the amount of steps taken in a sampling trajectory, as previously discussed. We want to define our standard unit of time here as pseudoseconds s. From here on $\tau = 2.5s$ and $\delta t = 0.1s$ for a total of 25 steps for each trajectory.
t_{max}	The total runtime of a simulation. From here on we will set this parameter to $t_{max} = 100s$ for a total of 1000 time steps. Once the system reaches a stable configuration this parameter does not have a significant influence on the simulation.
N_{traj}	The amount of virtual trajectories used to calculate the causal entropic force. This parameter needs to be sufficiently high, so we can assume that enough paths through phase space were taken and we get a good statistical approximation of the causal entropic force. It is set to $N_{traj} = 2500$ for all simulations.

Table 1: Table of simulation parameters.

6 Results

6.1 Order parameter

To quantify lane formation it is necessary to introduce the concept of an order parameter [3, 7, 8]. The definition of this parameter varies over different models. We first define a time and space dependent parameter: the local order parameter $\Theta(y,t)$, which we use to illustrate lanes in our plots and analyse the formation of lanes. Afterwards, we will define an averaged order parameter, the global order parameter Θ, to compare different parameters and their influence on lane formation. For the first parameter we want to look at steady-state, well formed lanes; for this we consider all pedestrians with y-coordinates in an interval $[y, y+\delta y]$. We define the number of pedestrians with preferred direction in the positive x-direction as $n_+(y,t)$, those with preferred direction in negative x-direction as $n_-(y,t)$. Now we can define the local order parameter as

$$\theta(y,t) \equiv \frac{n_+(y,t) - n_-(y,t)}{n_+(y,t) + n_-(y,t)}. \tag{38}$$

We immediately see the boundaries for this value as $-1 \leq \theta(y,t) \leq 1$. A value of 1 indicates a lane with preferred direction in positive x-direction, while a value of -1 indicates a lane with an opposite preferred direction. Values around 0 indicate a mixed state and thus a state without lanes. Plotting its dependence on t and y gives us an immediate visualisation of our lanes.

We now define the global order parameter

$$\Theta = \left\langle \frac{\langle |n_+(y,t) - n_-(y,t)| \rangle_y}{N_{total}} \right\rangle_t. \tag{39}$$

Here we average over time t after a transient of $t_{max}/2$. An order parameter $0 \leq \Theta \leq 1$ close to 0 denotes a completely mixed state without lane formation, while a global order parameter of 1 indicates a state of lane formation. This gives us a good indicator of lane formation for an entire simulation, which allows us to compare different parameter values.

6.2 Lane formation

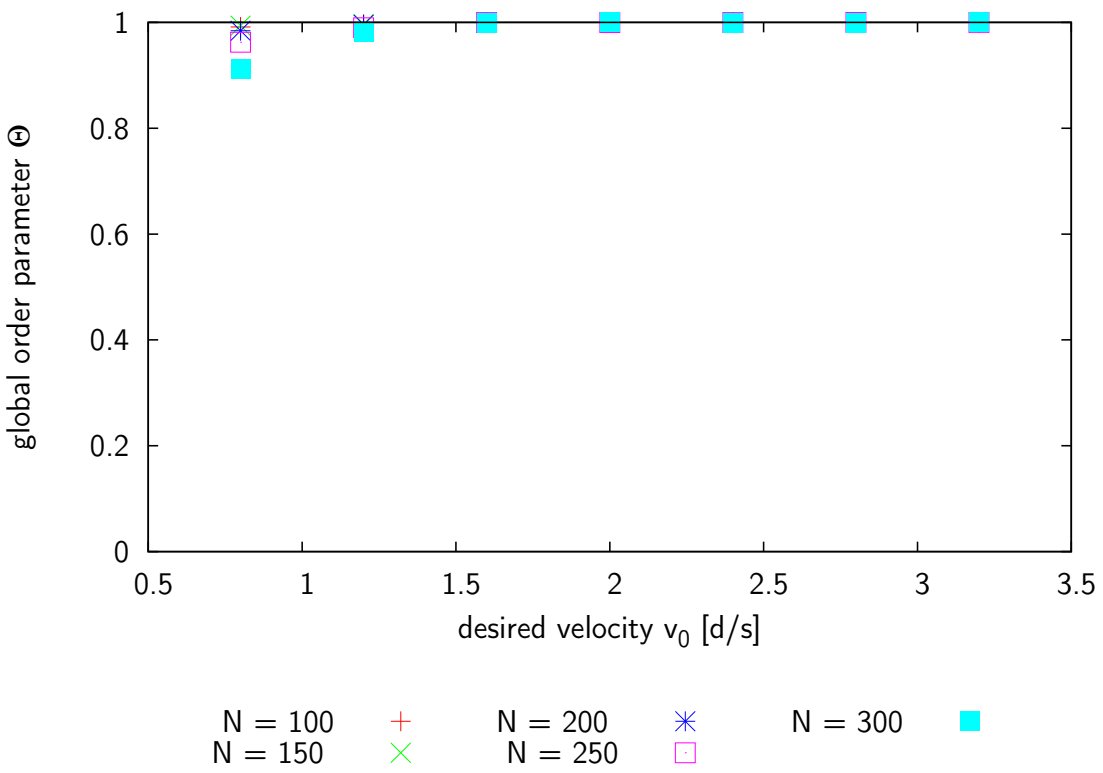

Figure 11: Global order parameter Θ with no causal entropic force for different desired velocities v_0 and different amounts of simulated pedestrians N.

First of all, we take a look at simulations with the causal entropic force turned off. We can use this as a baseline to compare values of the global order parameter Θ. In figure 11 we see the global order parameter Θ for different amounts of pedestrians N and different desired velocities v_0. We observe that Θ is close to 1 for the entire range of parameters shown in the plot. The order parameter increases slightly from $v_0 = 0.8d/s$ to $v_0 = 1.6d/s$, where it approaches unity for all N. With values consistently above $\Theta > 0.9$, Θ is still firmly in the range, where we expect lane formation to occur. This shows us that lane formation is achieved even without the causal entropic force, purely through the driving and friction term, as well as the harmonic potential between pedestrians.

Taking a closer look at snapshots of our simulations (see appendix figure 23) we find a large number of lanes with small width. Plotting the local order parameter should give us a better look at the formation and time evolution of these lanes. In figure 24 in the appendix we show the local order parameter for different y intervals and timesteps. Here we see the formation of stable lanes with uniform walking direction. We observe that for a higher velocity the systems reach stable

configurations much faster. Once the configuration reaches a stable state, it does not fluctuate and there are no lanes moving up or down in the channel. Plotting the

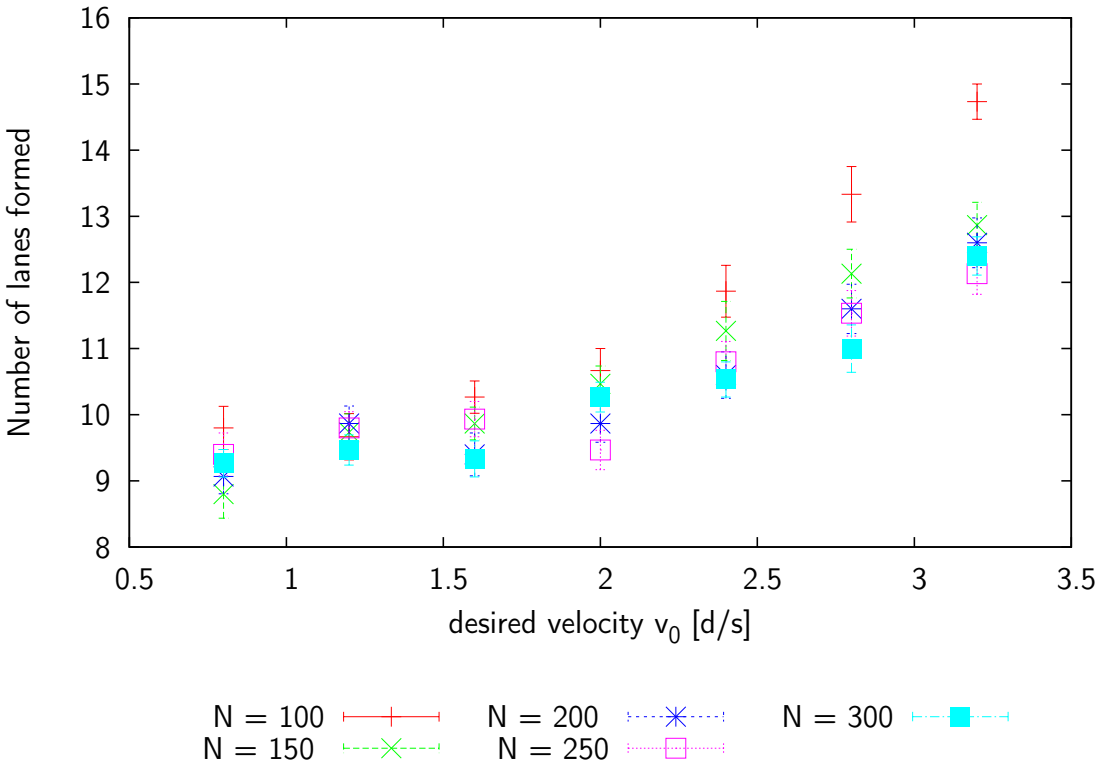

Figure 12: Average number of lanes formed for different desired velocities v_0 and different amounts of simulated pedestrians N without causal entropic force. Averaged over 30 simulations.

average number of lanes for different values of N and v_0 will give us a baseline to compare with the entropically driven simulations (see figure 12). Here we see that the average amount of lanes formed seems to be dependent both on the desired velocity v_0 as well as the amount of simulated pedestrians N. For velocities $v_0 \leq 2d/s$ the average amount of lanes formed is about 9 to 10. With larger desired velocities the number of lanes formed increases, with $N = 100$ simulated pedestrians forming the most lanes with almost 15 lanes on average. For all other N the number of lanes is within 0.5 to 1 of the number of lanes formed by simulations with $N \neq 100$, with a maximum difference of 1.13 between $N = 150$ and $N = 300$ simulated pedestrians at $v_0 = 2.8d/s$. From here on we want to take a closer look at $N = 150$ and $N = 250$ pedestrians. It is also noted that the difference in lanes formed between these two never exceeds 1.

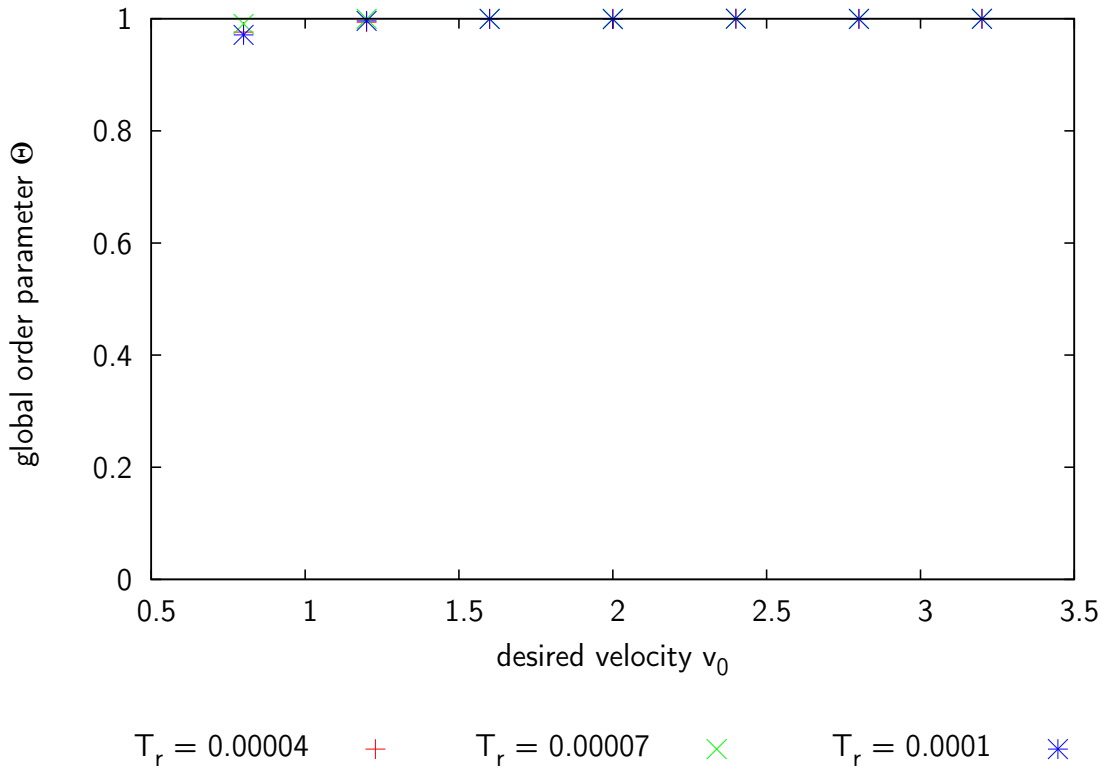

Figure 13: Global order parameter with causal entropic force for different desired velocities v_0 and different reservoir temperatures T_r. $T_c/T_r = 5$, $N = 150$, averaged over 10 simulations.

In figure 13 we see the global order parameter for entropically driven simulations with $N = 150$ pedestrians. We observe the same general behaviour as in the case without the causal entropic force. The order parameter does not drop below 0.9 again, which indicates lane formation. We also observe a steep increase in order parameter for lower desired velocities v_0 with $T_r = 0.00007$, with an order parameter of $\Theta = 0.97$ compared to the $\Theta \approx 0.9$ at $T_r = 0.00004$ and $T_r = 0.0001$.

In figure 14, where we set $N = 250$, we observe a significantly lower order parameter Θ for $v_0 < 1.2d/s$ with the highest reservoir temperature $T_r = 0.0001$ leading to the lowest order parameter. A lower reservoir temperature seems to lead to a higher order parameter for this velocity interval. For intermediate desired velocities the order parameter approaches unity as observed before in the other simulations. This further indicates lane formation.

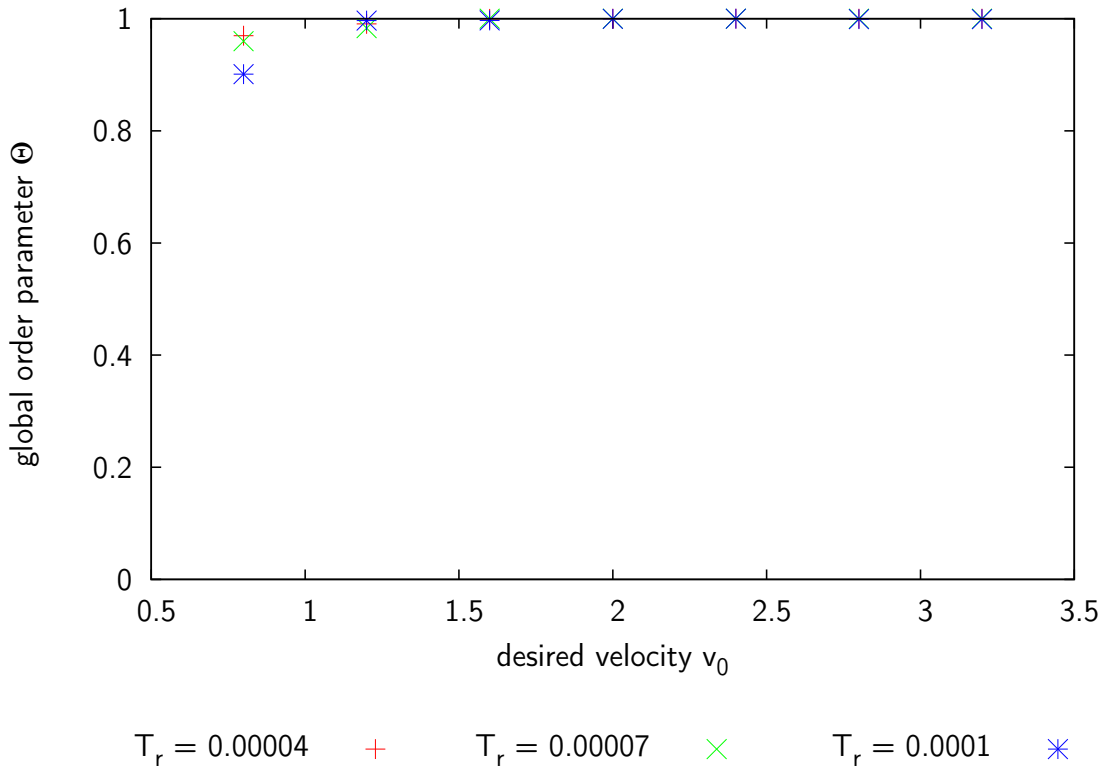

Figure 14: Global order parameter with causal entropic force for different desired velocities v_0 and different reservoir temperatures T_r. $T_c/T_r = 5$, $N = 250$, averaged over 10 simulations.

We again want to take a look at the local order parameter to confirm the formation of lanes and check the time evolution for simulations with the causal entropic force (see figure 25 in the appendix). We first look at the lowest order parameter encountered at $N = 250$, $T_r = 0.0001$ and $v_0 = 0.8d/s$. Here we observe the formation of 8 lanes of uniform walking direction. These lanes start forming very quickly at around 200 timesteps, while showing some instabilities until around 500 timesteps, with minor instabilities for the entirety of the simulation. The time until the lanes are formed is comparable to the simulations without the causal entropic force, while the observed instabilities are phenomena that did not occur at all in the simulations without the causal entropic force. For a larger desired velocity $v_0 = 3.2d/s$ we also observe the same minor instabilities, while the general formation of the lanes seems to be at a comparable speed to the simulations without the causal entropic force.

This seems to be a recurring phenomenon over all N, T_r and v_0 and these minor instabilities do not seem to break up lanes or hinder the formation of lanes. To further compare these simulations to those without the causal entropic force, we plot the average number of lanes for different amounts of pedestrians N as well as desired velocities v_0 and reservoir temperatures T_r(see figures 15, 16).

The average number of lanes formed for $N = 150$ pedestrians is comparable to the average number of lanes formed for the simulations without the causal entropic force and the same velocity dependence is observed. The average number of lanes formed for the simulations without the causal entropic force seem to be in the margin of error of the amount of lanes formed for both $N = 150$ and $N = 250$ pedestrians.

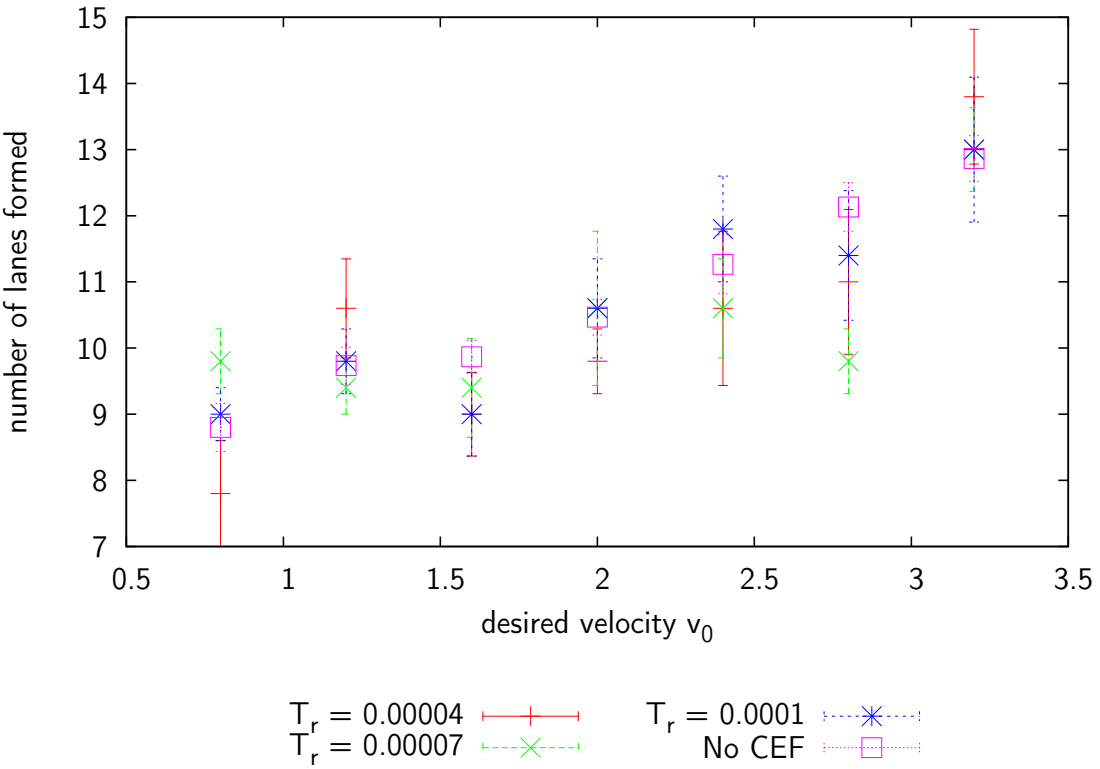

Figure 15: Average number of lanes formed for different desired velocities v_0 and different reservoir temperatures T_r. $T_c/T_r = 5$, $N = 150$, averaged over 10 simulations.

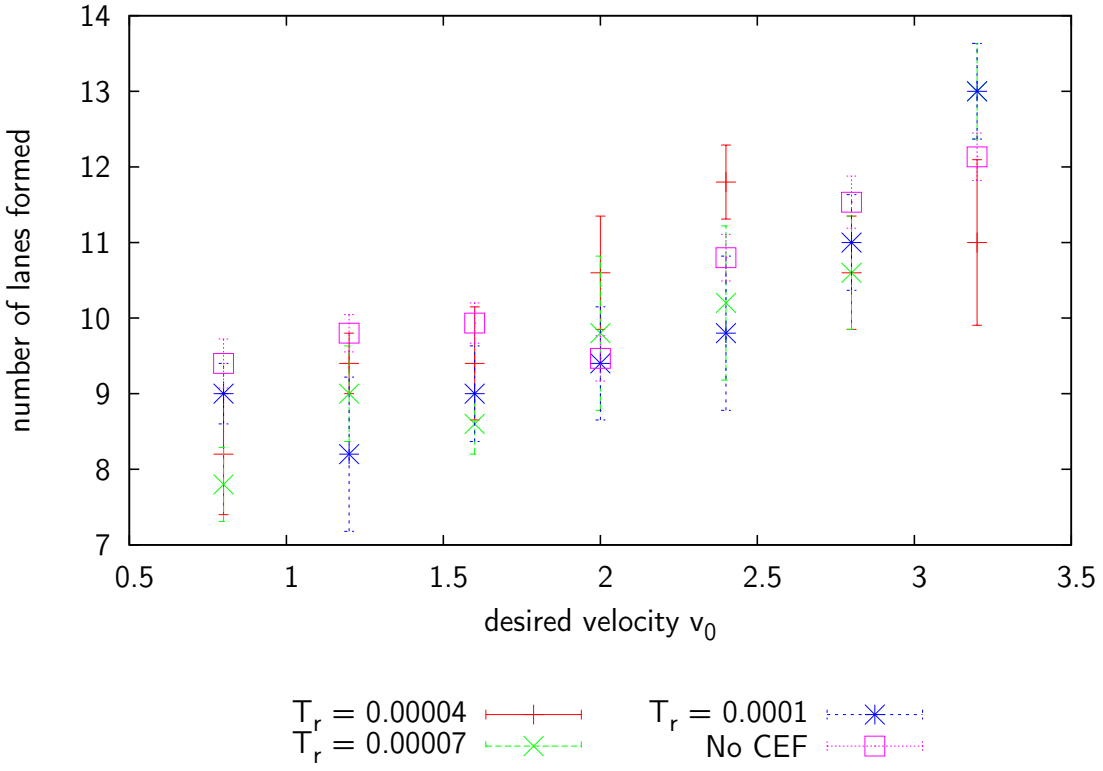

Figure 16: Average number of lanes formed for different desired velocities v_0 and different reservoir temperatures T_r. $T_c/T_r = 5$, $N = 250$, averaged over 10 simulations.

In the social force model a noise induced ordering effect would lead to a decrease in the amount of lanes formed [3]. The local order parameter plots have shown us that there are minor instabilities caused by the causal entropic force. To check whether these are similar in effect to the noise in the social force model, we increase the reservoir temperatures drastically in the following simulations. If the causal entropic force plays a similar role to the noise in the social force model we may observe an effect similar to the "freezing by heating" effect encountered in the social force model, leading to a blocking transition.

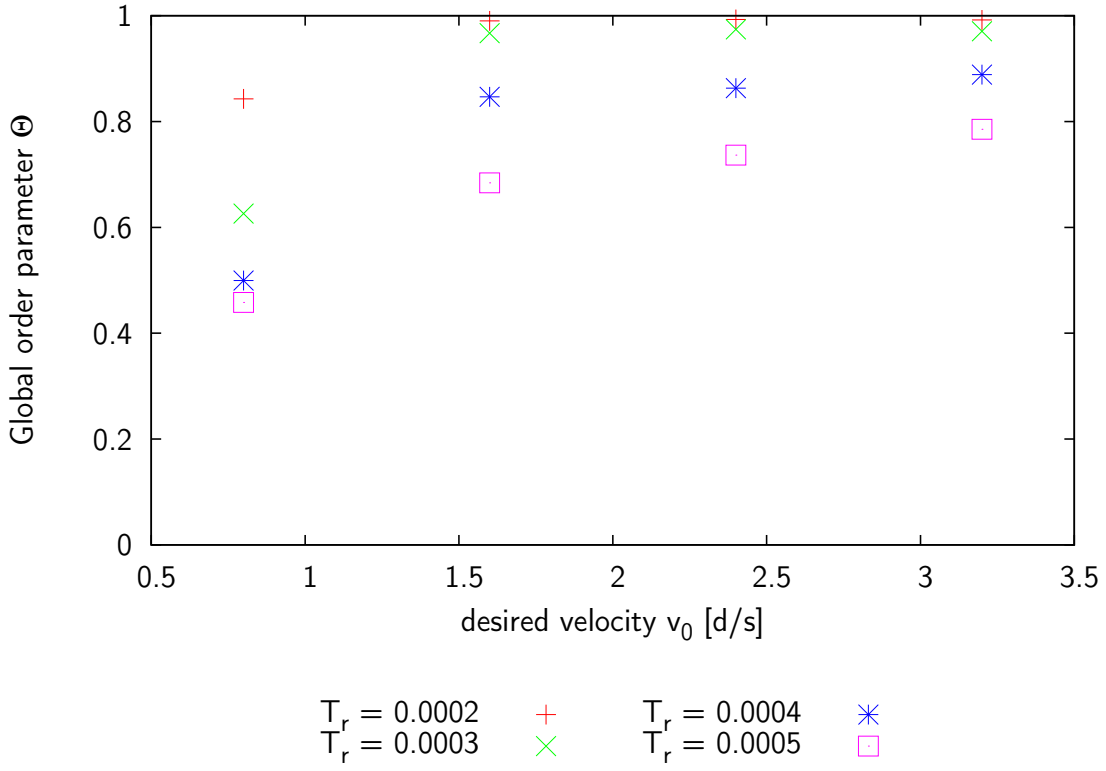

Figure 17: Global order parameter Θ for different desired velocities v_0 and different larger reservoir temperatures T_r. $T_c/T_r = 5$, $N = 150$, averaged over 10 simulations.

For larger reservoir temperatures T_r and $N = 150$ we observe a significant drop in order parameter for low velocities v_0 (see figure 17). Here $v_0 < 1d/s$ leads to order parameters below 0.7 with all reservoir temperatures except $T_r = 0.0002$. For all reservoir temperatures an increase in v_0 leads to a larger order parameter, with $T_r < 0.0004$ approaching 1. Reservoir temperature $T_r = 0.0004$ reaches order parameters between 0.8 and 0.9, while $T_r = 0.0005$ does not exceed an order parameter of 0.8. We take a look at the local order parameter for $T_r = 0.0005$ to analyse whether lane formation occurs for these parameters (see appendix figure 26).

We observe that, while there do seem to be lanes, they are highly unstable. We can, however, not observe a blocking transition here similar to the "freezing by heating" effect. We observe that a velocity of $v_0 = 1.6d/s$ leads to similar results, with the formation of highly unstable lanes. Lowering the velocity even further to $v_0 = 0.8d/s$ results in an essentially disordered state without any lanes. A reservoir temperature of $T_r = 0.0004$ at $v_0 = 3.2d/s$ seems to be right at the edge of the formation of stable lanes, with semi-stable lanes. These lanes however, compared to the lanes for the simulations with $T_r = 0.0005$, do not seem to split and the instabilities are confined to the edges of the lanes. One can argue that this is a sufficiently stable configuration as the amount of lanes formed does not change after

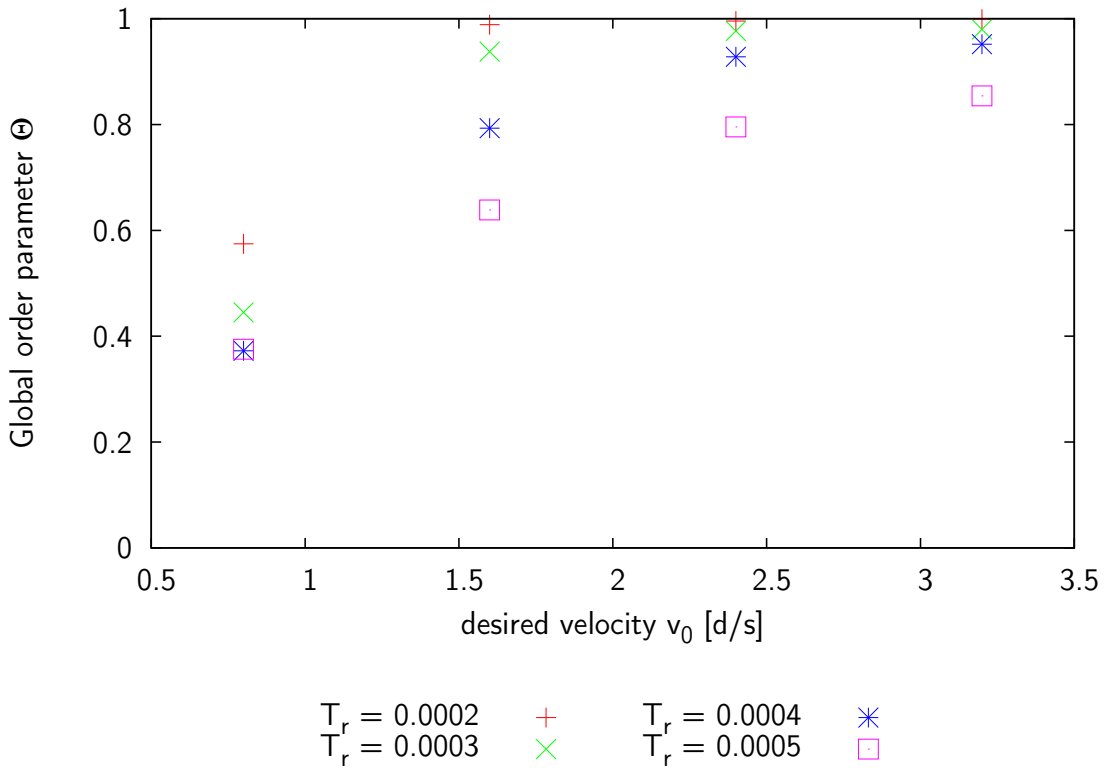

Figure 18: Global order parameter Θ for different desired velocities v_0 and different larger reservoir temperatures T_r. $T_c/T_r = 5$, $N = 250$, averaged over 10 simulations.

a transient. For $v_0 = 0.8d/s$ we do observe a disordered state, however this does not equate to a blocking transition as in the "freezing by heating" effect, as we still have movement into the preferred direction in our system.

For $N = 250$ simulated pedestrians (see figure 18) we observe the same general velocity dependence again, however for the higher density we observed a much larger global order parameter at all velocities for all reservoir temperatures. With $T_r = 0.0004$ exceeding $\Theta > 0.9$ at $v_0 = 2.4d/s$ and $T_r = 0.0005$ exceeding $\Theta = 0.8$ at $v_0 = 2.4d/s$.

The local order parameter plots (figure 27) show that lane formation, in contrast to the simulations of $N = 150$, is achieved through a higher pedestrian density. Here, at $T_r = 0.0005$ and $v_0 = 3.2d/s$ we still observe lane formation similar to the semi-stable lanes for $N = 150$ and $T_r = 0.0004$, and the amount of lanes again does not change after a transient period. The same is observed for $T_r = 0.0004$ and $v_0 \geq 2.4d/s$, with lanes breaking apart for lower desired velocities v_0.

We can conclude from this that the increase in density seems to have a rather large effect on the formation of lanes. This effect seems to be mostly present for large desired velocities, as the order parameter as well as the behaviour is essentially the same for lower desired velocities.

To analyse the amount of lanes formed in these simulations we first have to sort out the parameter ranges, where stable lanes have not formed. Because of the steep drop in order parameter we ignore all simulations at $v_0 = 0.8d/s$. As stable lanes do not form for $N = 150$ and $T_r = 0.0005$, we can rule out the entire $T_r = 0.0005$ parameter range for $N = 150$ pedestrians. With $T_r = 0.0004$ we observe the formation of unstable lanes for $N = 150$ simulated pedestrians with a velocity of $v_0 = 3.2d/s$. As stated before the amount of lanes does not change after a transient and we will thus include this parameter in our analysis of the amount of lanes formed. For $N = 250$ pedestrians we observed lane formation for $T_r = 0.0004$ and $v_0 \geq 2.4d/s$ as well as for $T_r = 0.0005$ and $v_0 = 3.2d/s$.

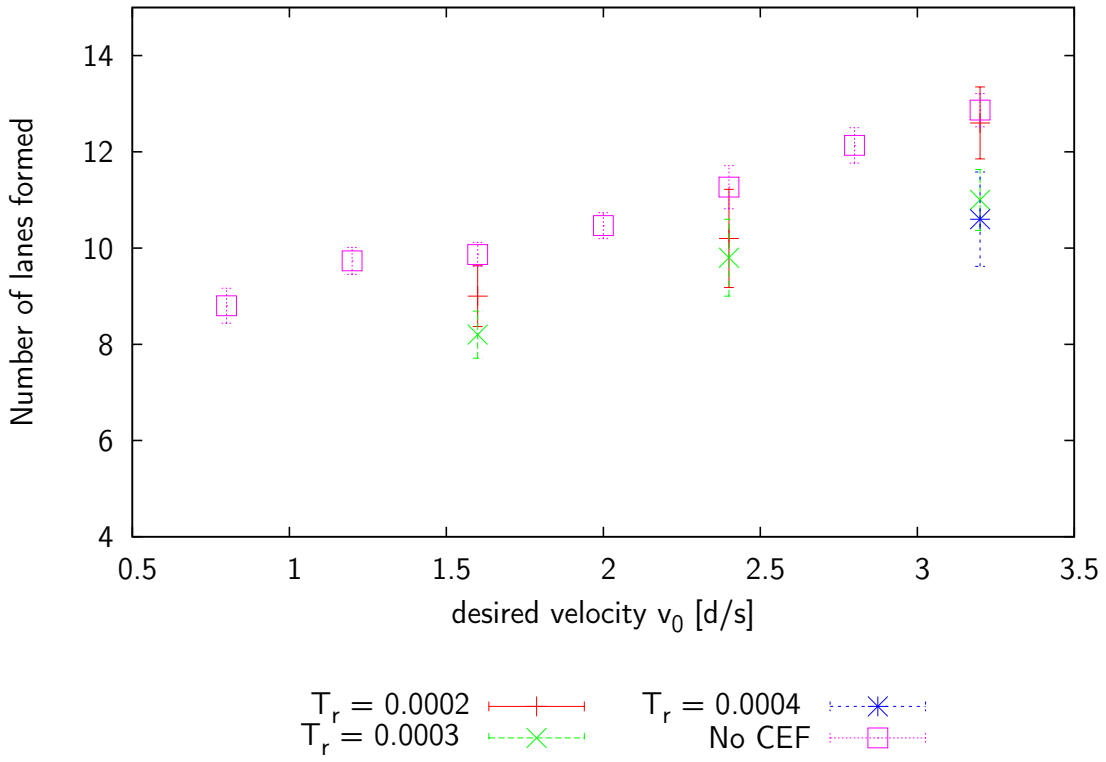

Figure 19: Average number of lanes formed for different desired velocities v_0 and different reservoir temperatures T_r. $T_c/T_r = 5$, $N = 150$, averaged over 10 simulations.

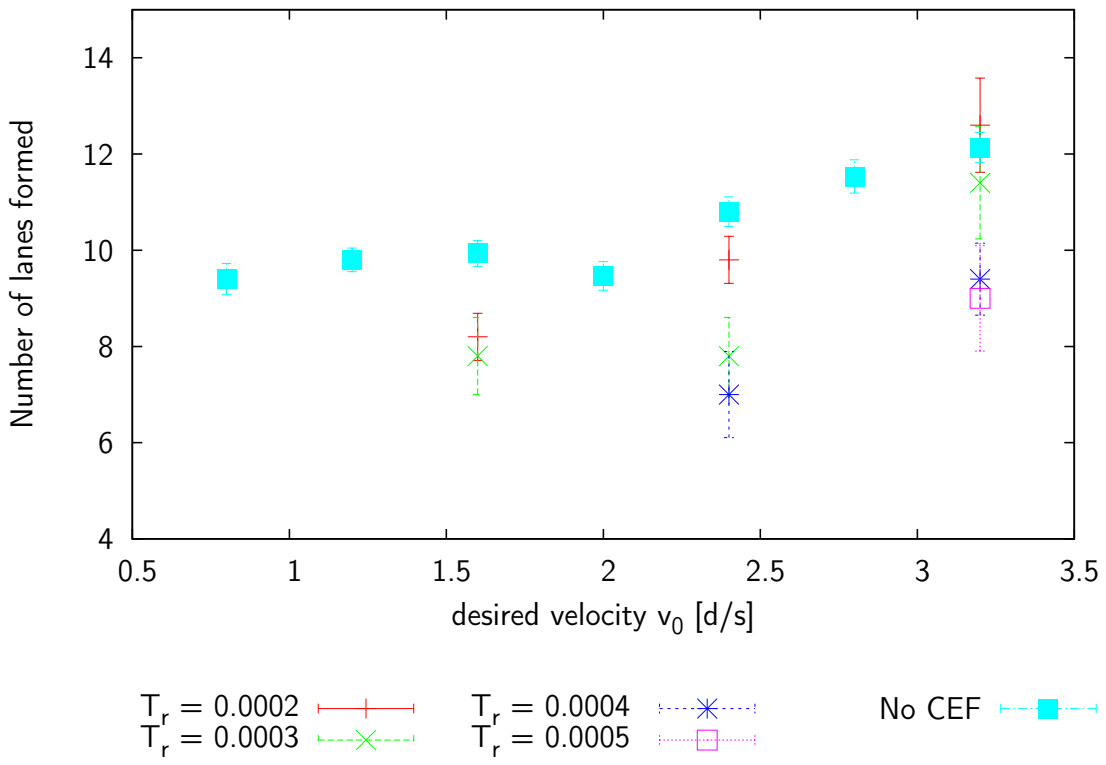

Figure 20: Average number of lanes formed for different desired velocities v_0 and different reservoir temperatures T_r. $T_c/T_r = 5$, $N = 250$, averaged over 10 simulations.

In figures 19 and 20 we see the amount of stable lanes formed for the valid parameter ranges. In both graphs we again observe that for all reservoir temperatures T_r a larger desired velocity v_0 will lead to more lanes formed. This is consistent with our findings for the intermediate values of T_r. We also observe that a larger reservoir temperature leads to fewer lanes formed, compared to other reservoir temperatures. This becomes more apparent for $T_r \geq 0.0004$, as these values are essentially at the border of the valid parameter range. Here we see huge differences of up to 3 fewer lanes. With our simulations at $T_r = 0.0005$, $N = 250$ and $v_0 = 3.2d/s$ forming on average only 9 ± 1.1 lanes formed, while the simulations without the causal entropic force form 12.1 ± 0.3 on average. This further indicates an ordering effect.

Taking a look at a snapshot from $T_r = 0.0005$, $v_0 = 0.8d/s$ and $N = 250$ (see figure 28) reveals a disordered state, however it does not resemble an ordered blocked state as one would expect from the "freezing by heating" effect. So we observe an ordering effect, indicated by the formation of fewer lanes by increasing the reservoir temperature, that does not lead to a blocking transition by further increasing the reservoir temperature.

6.3 Horizon comparison

To analyse the effect of the causal entropic force on our simulations we want to take a look at the horizon for different parameters. First of all we take a look at the horizons for low desired velocity v_0 and large reservoir temperature T_r.

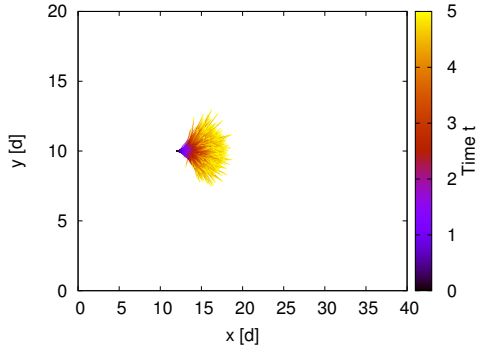

(a) Trajectory horizon for $v_0 = 0.8d/s$ and $T_r = 0.0001$

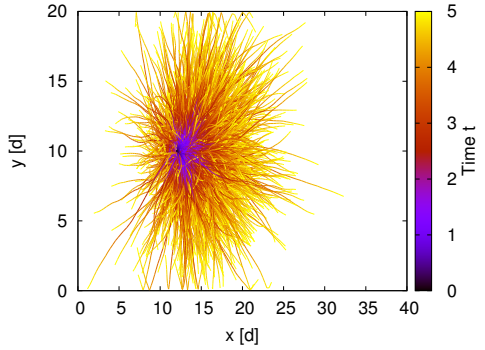

(b) Trajectory horizon for $v_0 = 0.8d/s$ and $T_r = 0.0005$

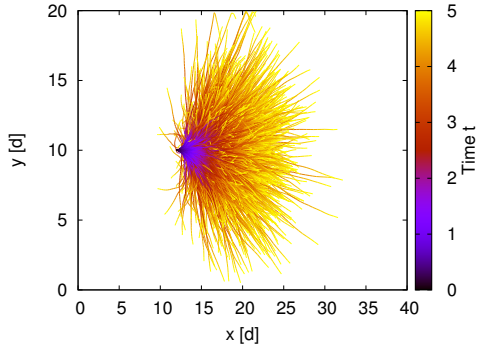

(c) Trajectory horizon for $v_0 = 1.6d/s$ and $T_r = 0.0004$

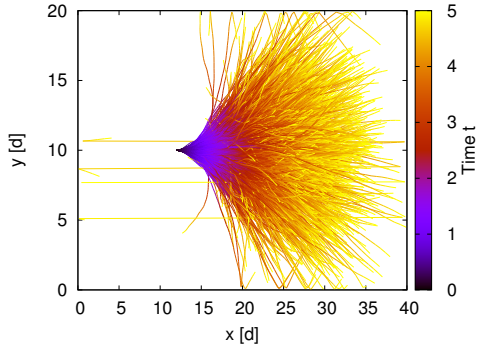

(d) Trajectory horizon for $v_0 = 3.2d/s$ and $T_r = 0.0005$

Figure 21: All plots show the trajectory horizon for different reservoir temperatures and desired velocities. In all plots the entire channel is shown to better compare the trajectory range.

In figure 21(a) we see the trajectory horizon for $T_r = 0.0001$ and $v_0 = 0.8d/s$. For these parameters we observed an order parameter Θ of over 0.9 for both $N = 150$ and $N = 250$. We observe a cone shaped form of the trajectory horizon. In figure 21(b) we see a more circular shape of the trajectory horizon with the distance covered in positive x-direction almost equaling the distance covered in y-direction. For $T_r = 0.0004$ and $v_0 = 1.6d/s$ (figure 21(c)) we did not observe lane formation in any simulation and again we observe a similar range in y-direction as in positive x-direction. In figure 21(d) we observed lane formation only for $N = 250$ but observe a more cone shaped form again. We conclude that the formation of lanes depends greatly on the envelop of the trajectory horizon. We can calculate the displacement

into the preferred direction of motion and the displacement because of causal entropy by considering a simple calculation. Taking a look at the formula for the interaction range (eq.37), the ratio of displacement in preferred direction of motion and the causal entropy displacement is

$$\frac{\tau v_0}{\frac{k_B T_r \sqrt{\tau dt}}{dt^2}} = \frac{\tau v_0 dt^2}{k_B T_r \sqrt{\tau dt}} \tag{40}$$

$$= \frac{1}{200} \frac{v_0}{T_r}; \tag{41}$$

in the last expansion we have plugged the numerical values used in the simulations. This calculation predicts that when $R \equiv \frac{v_0}{T_r}$ equals 200 we should expect considerable lane formation. We now plot the ratio R against the order parameter for $N = 150$ and $N = 250$ (see figure 22).

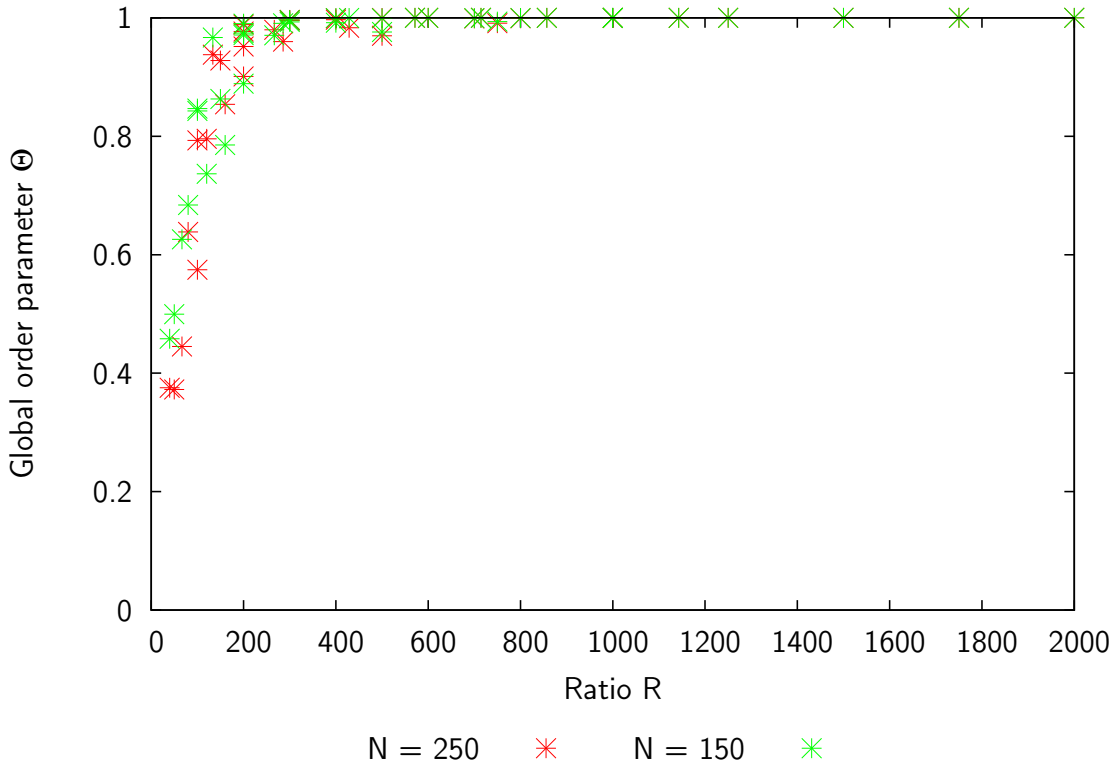

Figure 22: Ratio R of reservoir temperature and desired velocity for $N = 150$ and $N = 250$.

We observe indeed the order parameter Θ reaching unity for both values of N as the ratio $R = 200$, or larger values. We do not observe a large difference in the shape of the graph, as most order parameters were very similar for $N = 150$ and $N = 250$, with mostly qualitative differences in the formation of lanes.

7 Discussion and outlook

In conclusion, the driving and friction term coupled with the harmonic potential between pedestrians is enough for the segregation of pedestrians into stable lanes of uniform walking direction. The causal entropic force, at the right parameters, does not seem to break up these lanes. At intermediate values of the reservoir temperature T_r we did observe lane formation and the amount of lanes formed was within the margin of error of the simulation without the causal entropic force. By analysing the local order parameter we observed some minor instabilities as well as noise, which does not appear to destabilize the formation of lanes. The time until a stable configuration was reached was also comparable to the simulations without the causal entropic force.

Analysing large reservoir temperatures T_r confirmed that there is an ordering effect for large enough reservoir temperatures. Similar to the noise induced ordering in the social force model [3, 12, 14]. However in the social force model a blocking transition was observed by further increasing the noise, the "freezing by heating" effect. We however do not observe a blocking transition by increasing the reservoir temperature. Instead we observed segregation into short-lived unstable lanes. This indicates that the causal entropic force does not have the same effect on the system as the noise in the social force model. We compared the trajectory horizons and observed that a displacement of roughly the same distance covered in x-direction (or preferred direction of motion) and y-direction (or direction perpendicular to the preferred direction of motion) is the ratio at which lane formation occurs. Plotting this ratio revealed an almost monotone dependency of the global order parameter Θ on the ratio R, with Θ reaching unity at the calculated equal displacement at $R = 200$. We can conclude that the causal entropic force acts as an "intelligent noise".

The observed effects are a good indicator that the causal entropic force model may be able to accurately depict the dynamics of pedestrian flows. To further develop and analyse this simulation model, further phenomena of pedestrians flows, such as the oscillation of passing direction at bottlenecks, have to be simulated. Further work could also include the qualitative analysis of the $\frac{T_c}{T_r}$ ratio as well as a quantification of the ordering effect.

8 Appendix

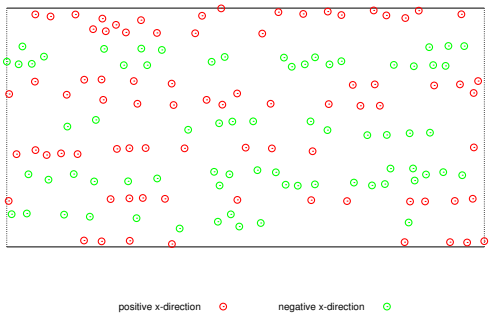

(a) $N = 150$, desired velocity $v_0 = 1.6d/s$, showing 9 lanes

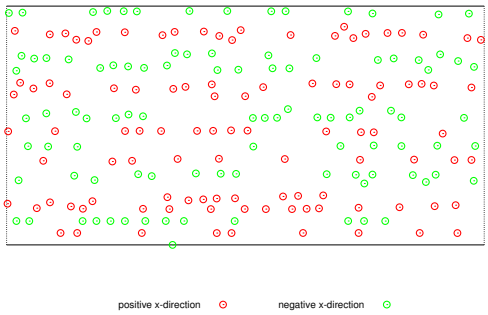

(b) $N = 200$, desired velocity $v_0 = 3.2d/s$, showing 13 lanes

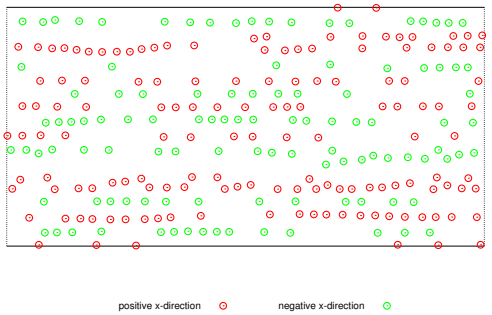

(c) $N = 250$, desired velocity $v_0 = 2.8d/s$, showing 15 lanes

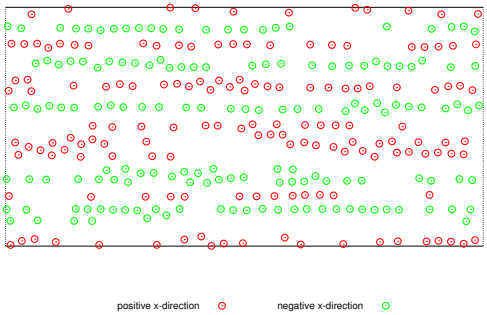

(d) $N = 300$, desired velocity $v_0 = 3.2d/s$, showing 11 lanes

Figure 23: All plots show snapshots of different simulations without the causal entropic force. Red circles denote pedestrians moving along positive x-direction, green circle denote pedestrians moving along negative x-direction. This shows the formation of lanes even without the causal entropic force.

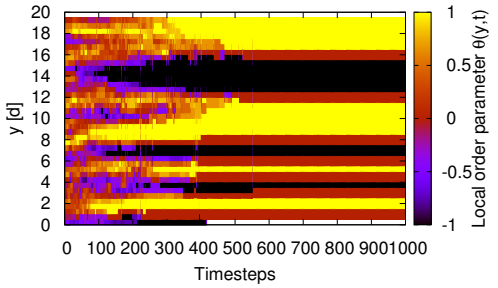

(a) $N = 150$, desired velocity $v_0 = 0.8d/s$, showing the formation of 7 stable lanes after around 500 timesteps

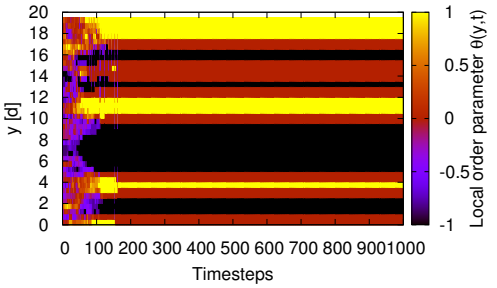

(b) $N = 150$, desired velocity $v_0 = 3.2d/s$, showing the formation of 7 stable lanes after around 150 timesteps

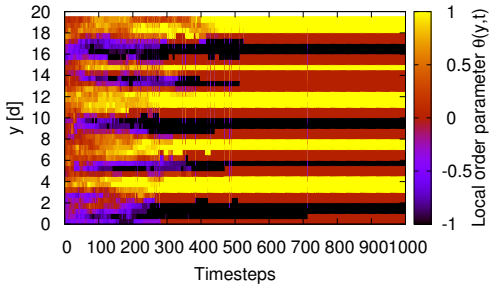

(c) $N = 250$, desired velocity $v_0 = 0.8d/s$, showing the formation of 9 stable lanes after around 500 timesteps

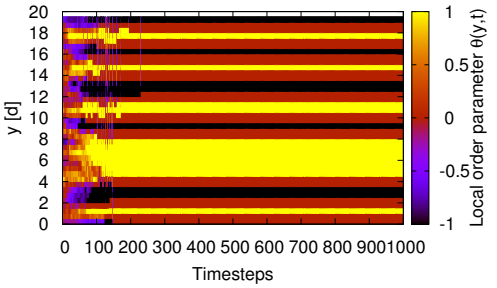

(d) $N = 250$, desired velocity $v_0 = 3.2d/s$, showing the formation of 10 stable lanes after around 250 timesteps

Figure 24: Plots of the local order parameter. The x-axis shows the time in timesteps, the y-axis shows the y-coordinate and the local order parameter is color-coded, with a value of 1 resulting in a preferred direction of movement along positive x-direction and a value of -1 resulting in a preferred direction of movement in negative x-direction.

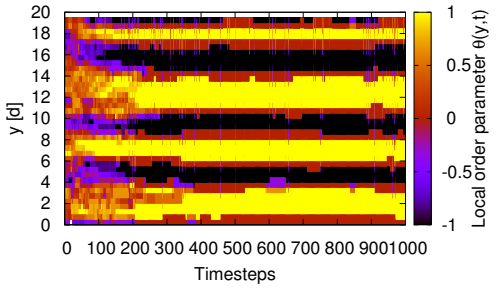

(a) $T_r = 0.0001$, $N = 150$, desired velocity $v_0 = 0.8d/s$

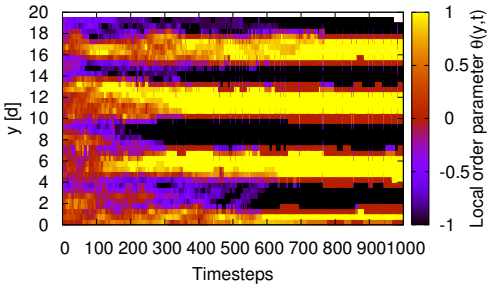

(b) $T_r = 0.0001$, $N = 250$, desired velocity $v_0 = 0.8d/s$

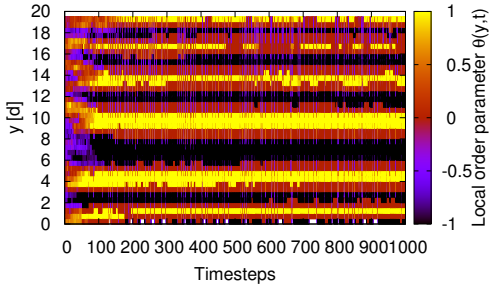

(c) $T_r = 0.0001$, $N = 250$, desired velocity $v_0 = 3.2d/s$

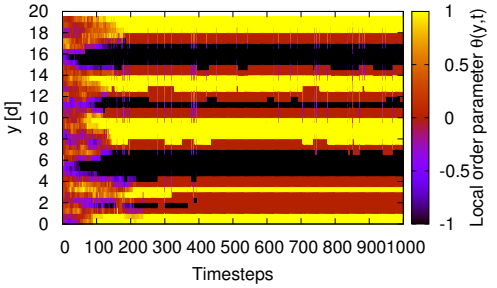

(d) $T_r = 0.00007$, $N = 250$, desired velocity $v_0 = 2.0d/s$

Figure 25: Plots of the local order parameter. The x-axis shows the time in timesteps, the y-axis shows the y-coordinate and the local order parameter is color-coded, with a value of 1 resulting in a preferred direction of movement along positive x-direction and a value of -1 resulting in a preferred direction of movement in negative x-direction.

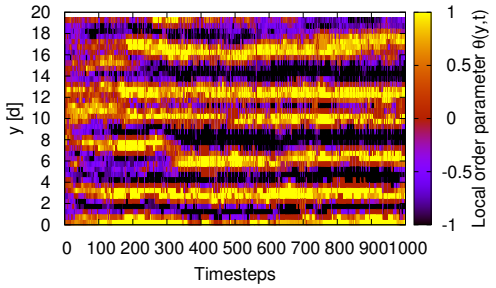

(a) $T_r = 0.0004$, $N = 150$, desired velocity $v_0 = 3.2d/s$

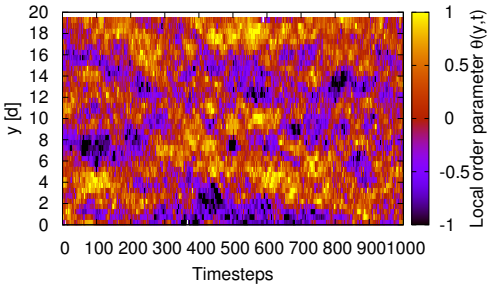

(b) $T_r = 0.0005$, $N = 150$, desired velocity $v_0 = 0.8d/s$

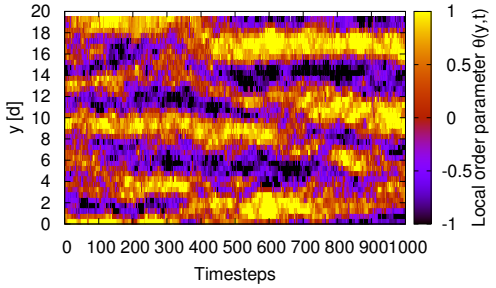

(c) $T_r = 0.0005$, $N = 150$, desired velocity $v_0 = 1.6d/s$

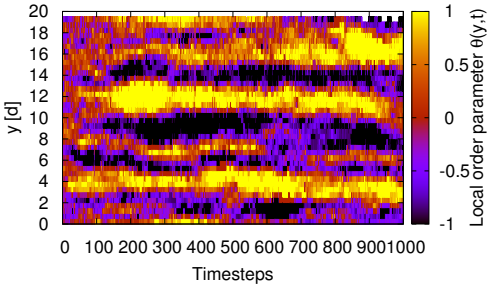

(d) $T_r = 0.0005$, $N = 150$, desired velocity $v_0 = 3.2d/s$

Figure 26: Plots of the local order parameter. The x-axis shows the time in timesteps, the y-axis shows the y-coordinate and the local order parameter is color-coded, with a value of 1 resulting in a preferred direction of movement along positive x-direction and a value of -1 resulting in a preferred direction of movement in negative x-direction.

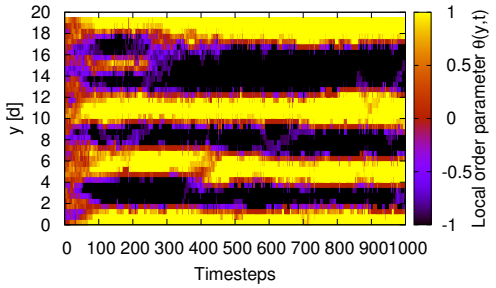

(a) $T_r = 0.0004$, $N = 250$, desired velocity $v_0 = 2.4d/s$

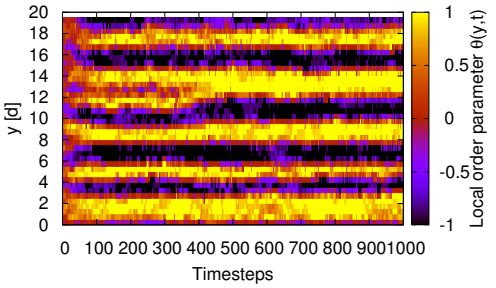

(b) $T_r = 0.0005$, $N = 250$, desired velocity $v_0 = 3.2d/s$

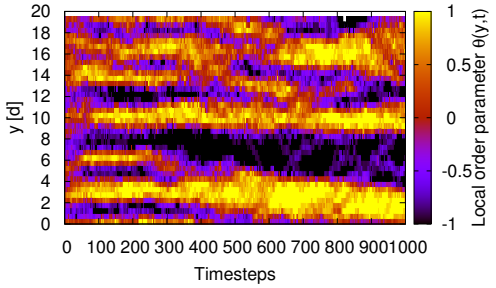

(c) $T_r = 0.0005$, $N = 250$, desired velocity $v_0 = 2.4d/s$

Figure 27: Plots of the local order parameter. The x-axis shows the time in timesteps, the y-axis shows the y-coordinate and the local order parameter is color-coded, with a value of 1 resulting in a preferred direction of movement along positive x-direction and a value of -1 resulting in a preferred direction of movement in negative x-direction.

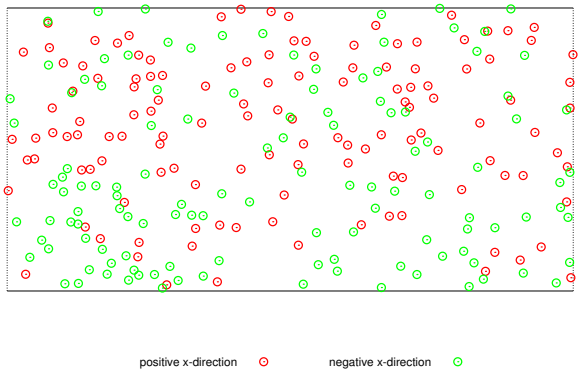

Figure 28: $N = 250$, reservoir temperature $T_r = 0.0005$, desired velocity $v_0 = 0.8d/s$, showing no formation of lanes

References

[1] A. D. Wissner-Gross and C. E. Freer, *Causal entropic forces*, Physical Review Letters **110**, 168702 (2013).

[2] X.-d. Liu, W.-g. Song, F.-z. Huo, and Z.-g. Jiang, *Experimental study of pedestrian flow in a fire-protection evacuation walk*, Procedia Engineering **71**, 343 (2014).

[3] D. Helbing, I. J. Farkas, P. Molnar, and T. Vicsek, *Simulation of pedestrian crowds in normal and evacuation situations*, Pedestrian and Evacuation Dynamics **21**, 21 (2002).

[4] H. Hornischer, *Causal entropic forces: Intelligent behaviour, dynamics and pattern formation*, Master's Thesis, Georg-August-Universität Göttingen (2015).

[5] D. Helbing and T. Vicsek, *Optimal self-organization*, New Journal of Physics **1**, 13 (1999).

[6] I. D. Couzin and N. R. Franks, *Self-organized lane formation and optimized traffic flow in army ants*, Proceedings of the Royal Society of London B: Biological Sciences **270**, 139 (2003).

[7] T. Vissers, A. Wysocki, M. Rex, H. Löwen, C. P. Royall, A. Imhof, and A. van Blaaderen, *Lane formation in driven mixtures of oppositely charged colloids*, Soft Matter **7**, 2352 (2011).

[8] J. Dzubiella, G. Hoffmann, and H. Löwen, *Lane formation in colloidal mixtures driven by an external field*, Physical Review E **65**, 021402 (2002).

[9] B. Schmittmann and R. Zia, *Phase transitions and critical phenomena*, Domb and J.L. Lebowitz Academic, New York **17** (1995).

[10] A. Schadschneider, H. Klüpfel, T. Kretz, C. Rogsch, and A. Seyfried, *Fundamentals of pedestrian and evacuation dynamics*, in *Multi-Agent Systems for Traffic and Transportation Engineering*, 124–154, (IGI Global 2009).

[11] S. P. Hoogendoorn and W. Daamen, *Pedestrian behavior at bottlenecks*, Transportation Science **39**, 147 (2005).

[12] D. Helbing, *Traffic and related self-driven many-particle systems*, Reviews of Modern Physics **73**, 1067 (2001).

[13] L. P. Kadanoff, *Simulating hydrodynamics: a pedestrian model*, Journal of Statistical Physics **39**, 267 (1985).

[14] D. Helbing and P. Molnar, *Social force model for pedestrian dynamics*, Physical Review E **51**, 4282 (1995).

[15] K. Yoshikawa, N. Oyama, M. Shoji, and S. Nakata, *Use of a saline oscillator as a simple nonlinear dynamical system: Rhythms, bifurcation, and entrainment*, American Journal of Physics **59**, 137 (1991).

[16] D. Helbing, J. Keltsch, and P. Molnar, *Modelling the evolution of human trail systems*, Nature **388**, 47 (1997).

[17] U. Weidmann, *Transporttechnik der fussgänger*, (IVT, Institut für Verkehrsplanung, Transporttechnik, Strassen-und Eisenbahnbau 1992).

[18] L. Henderson, *The statistics of crowd fluids*, Nature **229**, 381 (1971).

[19] H. C. Manual, *Special report 209*, Transportation Research Board, Washington, DC **1**, 985 (1985).

[20] J. S. Coleman and J. James, *The equilibrium size distribution of freely-forming groups*, Sociometry **24**, 36 (1961).

[21] D. Helbing, *Selbstorganisation kollektiver phänomene*, in *Verkehrsdynamik*, 37–44, (Springer 1997).

[22] J. P. Keating, *The myth of panic*, Fire Journal **76**, 57 (1982).

[23] D. Elliott and D. Smith, *Football stadia disasters in the United Kingdom: learning from tragedy?*, Organization & Environment **7**, 205 (1993).

[24] W. Predtetschenski and A. Milinski, *Personenströme in Gebäuden. Berechnungsmethoden für die Projektierung*, (Verlagsgesellschaft Rudolf Müller, Köln-Braunsfeld 1971).

[25] A. Mintz, *Non-adaptive group behavior*, The Journal of Abnormal and Social Psychology **46**, 150 (1951).

[26] R. A. Smith and J. F. Dickie, *Engineering for crowd safety: proceedings of the International Conference on Engineering for Crowd Safety, London, UK, 17-18 March, 1993*, (Elsevier Science Ltd 1993).

[27] D. Helbing, I. J. Farkas, and T. Vicsek, *Freezing by heating in a driven mesoscopic system*, Physical Review Letters **84**, 1240 (2000).

[28] D. Helbing, L. Buzna, A. Johansson, and T. Werner, *Self-organized pedestrian crowd dynamics: Experiments, simulations, and design solutions*, Transportation Science **39**, 1 (2005).

[29] R. Bousso, R. Harnik, G. D. Kribs, and G. Perez, *Predicting the cosmological constant from the causal entropic principle*, Physical Review D **76**, 043513 (2007).

[30] A. Kleidon, *Life, hierarchy, and the thermodynamic machinery of planet earth*, Physics of Life Reviews **7**, 424 (2010).

[31] L. Martyushev and V. Seleznev, *Maximum entropy production principle in physics, chemistry and biology*, Physics Reports **426**, 1 (2006).

[32] E. J. Chaisson, *Cosmic evolution: The rise of complexity in nature*, (Harvard University Press 2002).

[33] S. Gelly, L. Kocsis, M. Schoenauer, M. Sebag, D. Silver, C. Szepesvári, and O. Teytaud, *The grand challenge of computer Go: Monte Carlo tree search and extensions*, Communications of the ACM **55**, 106 (2012).

Erklärung nach §13(9)der Prüfungsordnung für den Bachelor-Studiengang Physik und den Master-Studiengang Physik an der Universität Göttingen:

Hiermit erkläre ich, dass ich diese Abschlussarbeit selbständig verfasst habe, keine anderen als die angegebenen Quellen und Hilfsmittel benutzt habe und alle Stellen, die wörtlich oder sinngemäß aus veröffentlichten Schriften entnommen wurden, als solche kenntlich gemacht habe.
Darüberhinaus erkläre ich, dass diese Abschlussarbeit nicht, auch nicht auszugsweise, im Rahmen einer nichtbestandenen Prüfung an dieser oder einer anderen Hochschule eingereicht wurde.

Göttingen, den 13. Januar 2017

(Florian Ebmeier)